Nano-Micro Letters

ISSN 2311-6706
e-ISSN 2150-5551
CN 31-2103/TB

REVIEW

https://doi.org/10.1007/s40820-019-0273-1

Cite as
Nano-Micro Lett.
(2019) 11:44

Received: 13 March 2019
Accepted: 23 April 2019
Published online: 25 May 2019

NASICON-Structured $NaTi_2(PO_4)_3$ for Sustainable Energy Storage

Mingguang Wu[1], Wei Ni[2,3] ✉, Jin Hu[1] ✉, Jianmin Ma[1,4] ✉

✉ Wei Ni, wei.ni@oulu.fi; Jin Hu, hujin@hnu.edu.cn; Jianmin Ma, nanoelechem@hnu.edu.cn

1 School of Physics and Electronics, Hunan University, Changsha 410082, People's Republic of China

2 Faculty of Technology, University of Oulu, 90014 Oulu, Finland

3 Panzhihua University, Panzhihua 617000, People's Republic of China

4 Key Laboratory of Materials Processing and Mold, Ministry of Education, Zhengzhou University, Zhengzhou 450002, People's Republic of China

HIGHLIGHTS

- For the first time, we fully presented the recent progress of the application of $NaTi_2(PO_4)_3$ on sodium-ion batteries including non-aqueous batteries, aqueous batteries, aqueous batteries with desalination, and sodium-ion hybrid capacitors.
- The unique NASICON structure of $NaTi_2(PO_4)_3$ and the various strategies on improving the performance of $NaTi_2(PO_4)_3$ electrode have been presented and summarized in detail.

ABSTRACT Several emerging energy storage technologies and systems have been demonstrated that feature low cost, high rate capability, and durability for potential use in large-scale grid and high-power applications. Owing to its outstanding ion conductivity, ultrafast Na-ion insertion kinetics, excellent structural stability, and large theoretical capacity, the sodium superionic conductor (NASICON)-structured insertion material $NaTi_2(PO_4)_3$ (NTP) has attracted considerable attention as the optimal electrode material for sodium-ion batteries (SIBs) and Na-ion hybrid capacitors (NHCs). On the basis of recent studies, $NaTi_2(PO_4)_3$ has raised the rate capabilities, cycling stability, and mass loading of rechargeable SIBs and NHCs to commercially acceptable levels. In this comprehensive review, starting with the structures and electrochemical properties of NTP, we present recent progress in the application of NTP to SIBs, including non-aqueous batteries, aqueous batteries, aqueous batteries with desalination, and sodium-ion hybrid capacitors. After a thorough discussion of the unique NASICON structure of NTP, various strategies for improving the performance of NTP electrode have been presented and summarized in detail. Further, the major challenges and perspectives regarding the prospects for the use of NTP-based electrodes in energy storage systems have also been summarized to offer a guideline for further improving the performance of NTP-based electrodes.

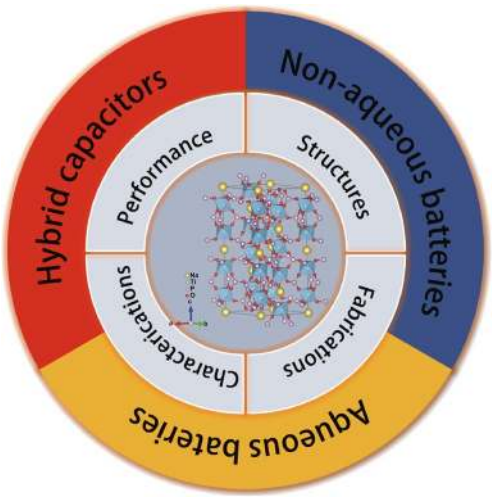

KEYWORDS $NaTi_2(PO_4)_3$; Sodium superionic conductor; Anode; Batteries; Hybrid capacitors

1 Introduction

In recent years, with the increasing consumption of fossil fuels, numerous studies have investigated the development of various types of renewable and clean energy devices [1–10]. Among current technologies, lithium-ion batteries (LIBs) have been considerably developed and widely used in portable electronic devices and large-scale grid storage applications because of their high energy density and long lifespan [11, 12]. However, the limited lithium resources and the rising cost of LIBs have stimulated research on the similar sodium-ion batteries (SIBs) on account of sodium's abundance in nature and environmental benignity [13–20]. At the same time, some other sodium-based energy devices such as aqueous batteries with desalination have also been developed due to their wide range of applications [21, 22].

Generally, both LIBs and SIBs rely on the reversible intercalation and deintercalation process of lithium or sodium ions between the positive and negative electrodes via the electrolyte during the charging and discharging process to complete energy conversion [13]. In particular, active electrode materials, especially anode materials, play an important role in the performance of batteries. In that regard, the development of suitable anode materials with high capacity, long cycle life, and excellent rate performance is of significant importance [15, 18, 23–28].

At present, although research on LIBs and SIBs has made considerable progress, and the most advanced batteries usually have high energy density, the slow kinetics of ion intercalation and deintercalation limits the achievement of higher power density and better rate performance [14, 25, 29].

Supercapacitors (SCs), characterized by electric double-layer capacitors (EDLCs), are a new type of energy storage device that stores energy by physical adsorption/desorption of an electric charge to form an electric double layer on the electrode-electrolyte interface. The excellent electrode dynamics of physical absorption and desorption enable features such as high power capability, excellent cycling performance, and long lifespan [30, 31]. However, EDLCs are inferior to batteries in terms of energy density [32, 33]. Therefore, merging the merits of the high-energy-density battery with the Faradaic electrode and high-power-density supercapacitor with the non-Faradaic electrode to develop a hybrid capacitor is a promising strategy to increase the energy density without sacrificing the high power density and long lifetime [30, 34–37].

Recently, NASICON (sodium superionic conductor) has gained tremendous attention as a promising anode material due to both its outstanding ion conductivity and high-voltage platform. The typical chemical formula of NASICON is $A_xMM'(XO_4)_3$, where A, M & M′, and X represent metallic elements (e.g., Li, Na, and K), transition metal elements (e.g., Ti, V, and Mn), and nonmetallic elements (e.g., P and S), respectively [25, 38–41]. Among these compounds, $NaTi_2(PO_4)_3$ (NTP) with an open framework is considered to be the optimal electrode material for SIBs due to its 3D open framework, in which TiO_6 octahedra share all corners with PO_4 tetrahedra, thereby providing a large interstitial space for Na^+ ion diffusion as shown in Fig. 1a [25, 32]. In recent years, many studies on the application of NTP in SIBs, including non-aqueous batteries, aqueous batteries, aqueous batteries with desalination, and sodium-ion hybrid capacitors, have been reported (see the typical examples in Tables S1 and S2) [42]. For example, one limitation of the present electrochemical system that is observed in full cells is capacity fade at low rates less than 1 C. By demonstrating high rate capability upon removal of the electronic conductivity limitation, the state-of-the-art results show that NTP has sufficiently high sodium chemical diffusivity to provide 100 C rate capability at submicron crystallite sizes, i.e., up to 70% of the NTP capacity can be obtained with a discharge time of 36 s. The aqueous Na-ion system, e.g., NTP/NMO, is capable of exceptionally high charge/discharge rates (over 100 C) and stable cycling to > 1000 cycles, while delivering severalfold higher energy densities than supercapacitors [43]. Moreover, some new Na-ion hybrid capacitor (NHC) systems with organic electrolytes could deliver a high energy density of, e.g., ≈ 80 Wh kg^{-1} and a high specific power of, e.g., 8 kW kg^{-1} without specific energy loss at a high voltage up to 3.0 V. An ultralow performance fading of, e.g., ≈ 0.13% per 1000 cycles (90%–75,000 cycles) outperforms previously reported results. Also, the enhanced charge transfer kinetics and reduced interfacial resistance at high current rates deliver high specific energy without compromising the high specific power along with high durability, and thereby bridge the batteries and capacitors. Thus, kinetically enhanced NHCs can be a trendsetter for the development of advanced energy storage devices requiring high energy and high power. The future prospects are promising, as most

https://doi.org/10.1007/s40820-019-0273-1

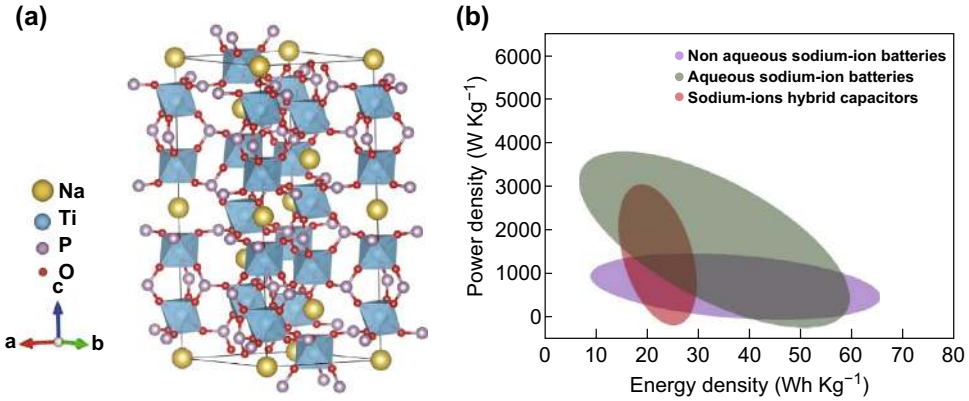

Fig. 1 **a** Crystal structure of $NaTi_2(PO_4)_3$ and **b** Ragone plot of $NaTi_2(PO_4)_3$-based materials for non-aqueous sodium-ion batteries, aqueous sodium-ion batteries, and sodium-ion hybrid capacitors [32, 43, 44, 46, 95, 127, 131, 132, 159, 164, 165, 218]

technical and product indexes, including the cycling stability, rate capabilities, weight loading, and cost of rechargeable SIBs and NHCs, have been raised to a commercially acceptable level as competitive alternatives to LIBs or capacitors. The Ragone plot of $NaTi_2(PO_4)_3$-based non-aqueous SIBs, aqueous SIBs, and sodium-ion hybrid capacitors is shown in Fig. 1b.

A systematic overview of the emerging critical progress is an urgent necessity. In this review, we will cover the recent progress in NTP-based electrodes for both NIBs and NHCs. The underlying synthesis methods, materials modification strategies, and electrochemical properties will be summarized in detail. Further, the major challenges and perspectives regarding the prospects for the use of NTP-based electrodes in energy storage systems will be summarized.

2 Sodium-Ion Batteries

NASICON-structured $NaTi_2(PO_4)_3$ has attracted increasing attention as a promising anode material due to the specific "zero-stress" framework with high Na-ion conductivity, long-term cycling stability, excellent rate capability, large theoretical capacity (133 mAh g^{-1}) as well as low cost, environmentally benignity, and much better safety characteristics [25, 43–49]. The reversible (de)sodiation between $NaTi_2(PO_4)_3$ and $Na_3Ti_2(PO_4)_3$, i.e., the redox reactions of $Ti^{3+} \leftrightarrow Ti^{4+}$ via a two-phase reaction mechanism, can be represented by Eq. (1) [44, 45]:

$$NaTi_2\left(PO_4\right)_3 + 2Na^+ + 2e^- \leftrightarrow Na_3Ti_2\left(PO_4\right)_3 \quad (1)$$

During discharge, the Na atom on Na_2 sites is reversibly removed while the Na_2 sites remain unaffected.

2.1 Non-aqueous Batteries

Delmas et al. first reported the reversible sodiation of $NaTi_2(PO_4)_3$ in an organic electrolyte and revealed that two Na^+ ions could be reversibly intercalated to form $Na_3Ti_2(PO_4)_3$ via a two-phase mechanism [50] showing a pair of typical well-defined redox peaks at 2.2/2.0 V within the potential window of 1.6–2.6 V (vs. Na/Na^+) [44], and a number of research groups conducted a detailed structural elucidation of the electrochemical transition and structural control related to this compound [51–56]. To enhance the inherent low electronic conductivity of the phosphate framework especially for high-power SIBs application, numerous efforts have been made to improve its electrochemical performance by nanoarchitecturing the NTP particles and incorporating conductive carbon coating/networks (e.g., amorphous carbon, CNTs, or graphene) [45, 48, 57–63].

2.1.1 Nanoarchitectures of NTP

Nanostructured NTP with higher surface areas usually has a higher capacity; e.g., it was reported by Niu and his coworkers that NTP nanoparticles synthesized by a pyro-synthetic reaction in comparison to that by a traditional solid-state method show a much higher surface area and better electrochemical performance: the rapid pouring of the homogeneous starting precursors onto the hot plate resulted in rapid precursor decomposition and subsequent nucleation of nanoparticles [64]. Yang et al. synthesized a high-rate non-aqueous SIB anode material of porous NTP nanocubes

with an over 10,000-cycle lifespan (75.5% retention of the initial capacity at a 10 C rate) (Fig. 2a, c). The controllable synthesis of porous NTP nanocubes with high regularity and porosity via a one-pot solvothermal route through the long-range oriented attachment of tiny nanocrystals into the 3D architectures (i.e., oriented attachment growth) will enrich the NTP system and provide several possible candidates for promising SIB anodes. The as-synthesized porous nanocubes showed excellent high rate performance and could still deliver considerable reversible capacities after deep charging/discharging over 15,000 cycles at an extremely high rate of 100 C. Ex situ TEM and XRD analyses further supported the conclusion that the electrochemical performance of NTPs is completely reversible upon Na^+ intercalation (Fig. 2b), ensuring robust structural stability and long cycle life for practical applications [48].

Crystalline order or the degree of crystallinity in NTP also plays an important role in electrochemical properties such as capacity and electrode kinetics. Ko et al. studied the correlation of electrochemical performance with crystalline order. Starting with an amorphous NTP powder prepared by the Pechini method, varied NTP nanoparticulates of different degrees of crystallinity were derived via calcination. It was observed that poorly crystalline NTP samples (derived at 500–600 °C) exhibited low specific capacities and broad voltammetric features for Na^+ insertion, characteristic of surface-limited processes; and highly crystalline NTP samples (derived at 700–800 °C) with the well-formed NASICON structure exhibited sharp voltammetric peaks and diffusion-limited kinetics in both organic (i.e., non-aqueous) and aqueous electrolytes. Further integration of nanocrystalline NTP with conductive networks can enhance the local electronic conductivity to a theoretical specific capacity in a non-aqueous electrolyte and an adequate capacity in a mildly aqueous electrolyte with significantly improved long-term stability [65].

2.1.2 Nanolayer-Coated NTP

Methods for the incorporation of carbon with $NaTi_2(PO_4)_3$ vary from carbon layer coating [60, 66–70], electrospinning [71–76], solvothermal synthesis [49, 62, 77], pyrosynthesis [64, 78], spray-drying [74], and assembly [79] to ball milling [80] for different morphologies or structures, e.g., porous plates [77], 1D nanofibers [71, 72], nanocubes [49, 73], mesoporous materials [67, 73], and hierarchical nanocomposites [60, 79]. Some related works about carbon-coated architectures have reported excellent or enhanced performance; e.g., the nanosized porous carbon-coated NTP particles prepared by He et al. through a hydrothermal process combined with various carbon coating steps showed superior rate (capacities of 106 mAh g^{-1} at 10 C over 1000 cycles, 111 mAh g^{-1} at 30 C) and low-temperature properties (98 mAh g^{-1} at 10 C and 61 mAh g^{-1} at 20 C even at − 20 °C). This indicated that the addition of a small amount of $Na_3Ti_2(PO_4)_3$ (NVP) intermediate powder accounts for the in situ catalytic formation of more sp^2-type carbon coating, i.e., highly graphitic carbon (graphene-like layers) coating, for excellent electrochemical performance of high-power SIBs [73].

Zhang et al. synthesized an open holey-structured framework for an NTP/C nanocomposite with open channels in nanocube morphologies for faster Na-ion transport by using a solvothermal reaction followed by pyrolysis. It demonstrated fast Na-ion transport and preferable battery performance, with a very small capacity decrease from 124 to 120 mAh g^{-1} in the wide range 0.5–50 C. An excellent discharge capacity of 103 mAh g^{-1} (88.3% retention of the first cycle) was delivered after an ultralong lifespan of 10,000 cycles at a super-high rate of 50 C [49]. Pang et al. synthesized a mesoporous $NaTi_2(PO_4)_3$/CMK-3 (NTP/C) nanohybrid with high-crystallinity NTP nanoparticles (size of ~ 5 nm) homogeneously embedded in the highly conductive mesoporous CMK-3 matrix via a solvothermal route followed by calcination. The CMK-3 not only served as a rigid, interconnected conductive support but also suppressed agglomeration or overgrowth of NTP nanoparticles. Even over 1000 cycles, the nanohybrid showed an integral structure with a well-crystallized rhombohedral $NaTi_2(PO_4)_3$ phase (Fig. 2d). Further, the nanohybrid anode showed some typical characteristics including a pair of well-defined sharp and stable redox peaks (located at 2.09 and 2.16 vs. Na^+/Na corresponding to the redox reaction of Ti^{4+}/Ti^{3+} during the reversible insertion–extraction reaction of Na^+ in the NTP lattice), high initial charge–discharge capacities (corresponding to a 75% utilization of its theoretical capacity with a high coulombic efficiency (CE) of 98% in the potential voltage window 1–3 V), and enhanced rate capabilities (with distinct charge–discharge voltage plateaus) compared to pure NTP at the same rate (Fig. 2e–g), which can be attributed to

 https://doi.org/10.1007/s40820-019-0273-1

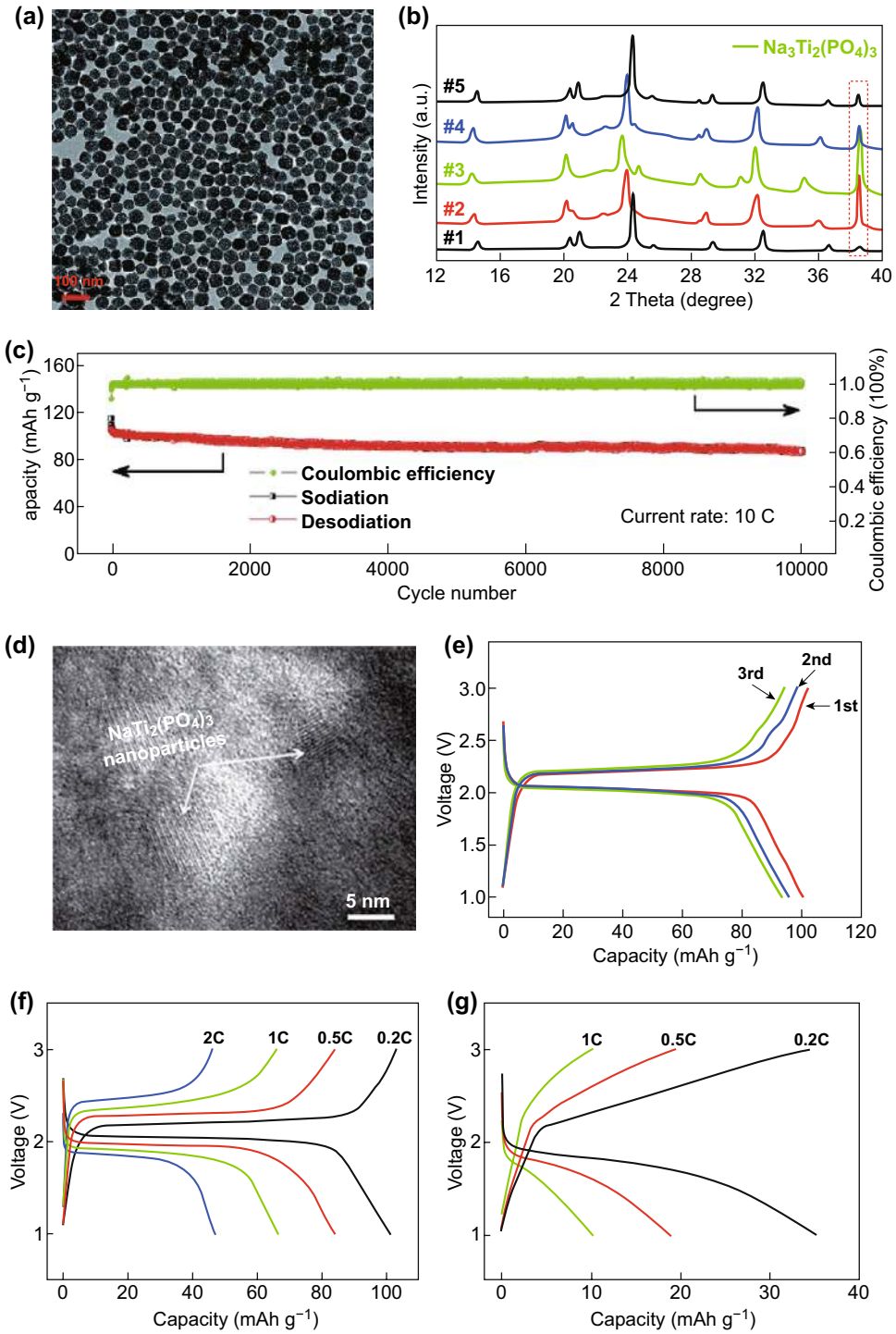

Fig. 2 a TEM image of typical NTP nanocubes obtained via a one-pot solvothermal method. **b** XRD diffraction patterns recorded at different stages of NTP upon charging/discharging. The diffraction peak marked with a dark-wine-red-dashed box in **b** corresponds to the aluminum current collector. **c** Cycling performance of NTP electrodes obtained at current rates of 10 C [48]. Copyright 2015, the Royal Society of Chemistry. **d** HRTEM images of the mesoporous NTP/CMK-3 nanohybrid electrode after 1000 cycles at the rate of 0.5 C. **e** The first three charge–discharge profiles of the NTP/C electrode at 0.2 C. **f** Galvanostatic charge–discharge (GCD) plots of NTP/C and **g** pure NTP anodes at various C-rates [58]. Copyright 2014, the Royal Society of Chemistry. (Color figure online)

the fast Na^+ insertion–extraction kinetics and good electrical conductivity of the mesoporous hybrid architecture [58].

Ma and coworkers prepared porous $NaTi_2(PO_4)_3$@C nanocubes (Fig. 3a, b) via a hydrothermal route followed by carbon coating using oleic acid as the carbon source. When utilized as an SIB anode, the mesoporous nanocubic hybrid could deliver an enhanced capacity of 201 mAh g^{-1} at 100 mA g^{-1} after 100 cycles, high rate capabilities, and a long cycle capacity of 140 mAh g^{-1} at 1.0 A g^{-1} over 1000 cycles in the voltage window 0.01–3.0 V (Fig. 3c–e) [81].

The extended work voltage below 1.0 V of the multi-step process, corresponding to $Ti^{3+} \leftrightarrow Ti^{2+}$, can be described by Eq. (2) [51, 69, 81]:

$$Na_3Ti_2(PO_4)_3 + Na^+ + e^- \leftrightarrow Na_4Ti_2(PO_4)_3 \quad (2)$$

which theoretically contributes an additional specific capacity of 119 mAh g^{-1} (i.e., with a total theoretical capacity of up to 252 mAh g^{-1} for $Na_3Ti_2(PO_4)_3$ in the voltage window 0–3 V vs. Na^+/Na) with a pair of primary redox peaks at a voltage as low as approximately 0.44 V [78], although in the

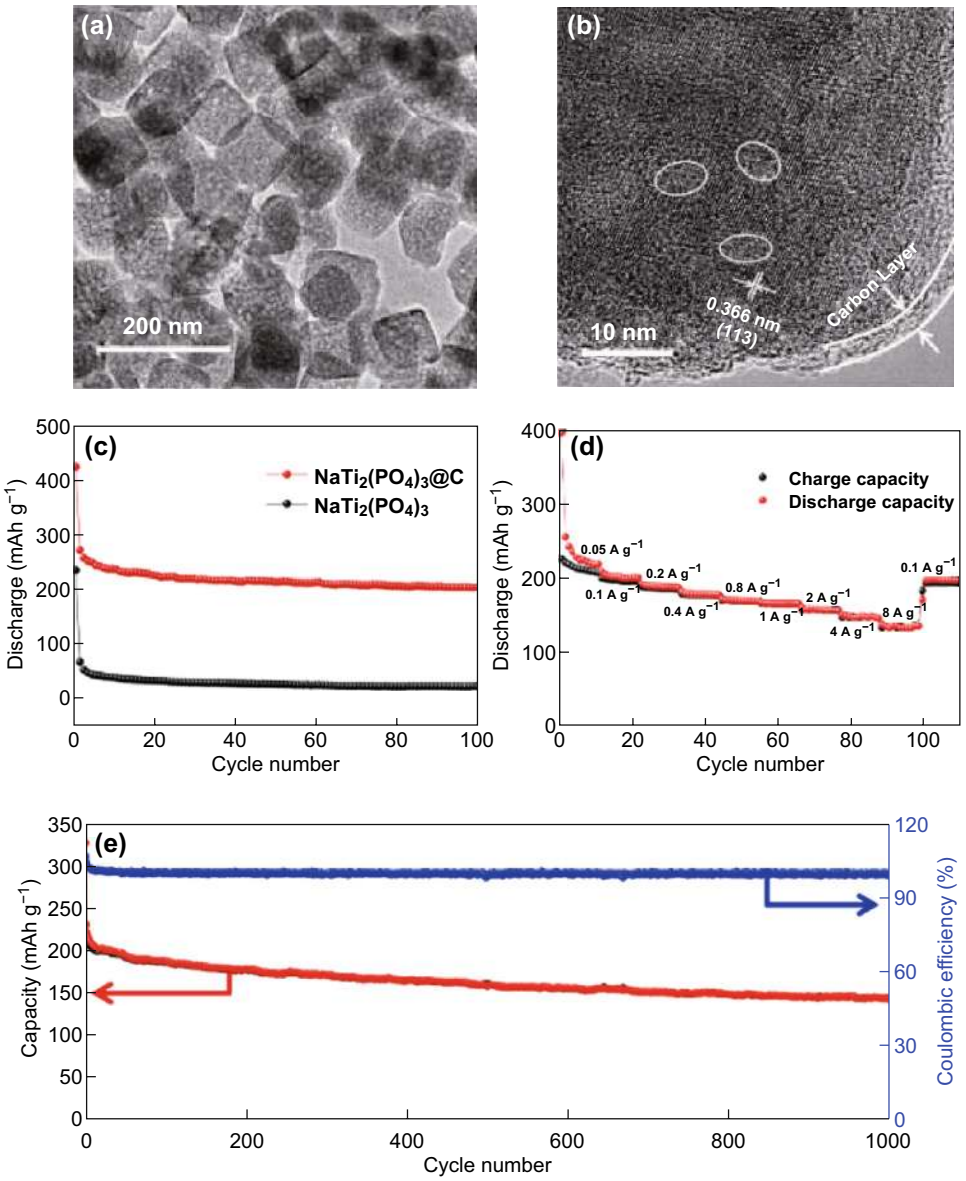

Fig. 3 **a**, **b** TEM images of $NaTi_2(PO_4)_3$@C. **c** Cycling performances of $NaTi_2(PO_4)_3$@C and $NaTi_2(PO_4)_3$ at 100 mA g^{-1}. **d** Rate capabilities of $NaTi_2(PO_4)_3$@C and **e** cycling performance of $NaTi_2(PO_4)_3$@C at the higher current density of 1 A g^{-1} [81]. Copyright 2017, Elsevier Ltd

 https://doi.org/10.1007/s40820-019-0273-1

first discharge process, a solid electrolyte interphase (SEI) will form below 1.5 V via consumption of extra Na^+ in the electrolyte, and the cyclability may deteriorate [69, 81–83]. Mai and coworkers designed an architecture comprising carbon-coated hierarchical NTP mesoporous microflowers (Fig. 4a, b) via a facile and controllable solvothermal route followed by annealing. The unique structure endows the hierarchical composite with outstanding structural stability, enhanced charge transfer kinetics, and suppressed polarization. It demonstrated a superior Na storage performance with a high initial capacity of 125 mAh g^{-1} at 1 C, an excellent rate capability of 95 mAh g^{-1} that is high even up to 100 C, and an ultralong cycling stability (77.3% capacity retention, i.e., 85 mAh g^{-1}, even after 10,000 cycles at 20 C) (Fig. 4g). A time-resolved in situ X-ray diffraction study (Fig. 4c–f) reveals the typical two-phase electrochemical reaction with

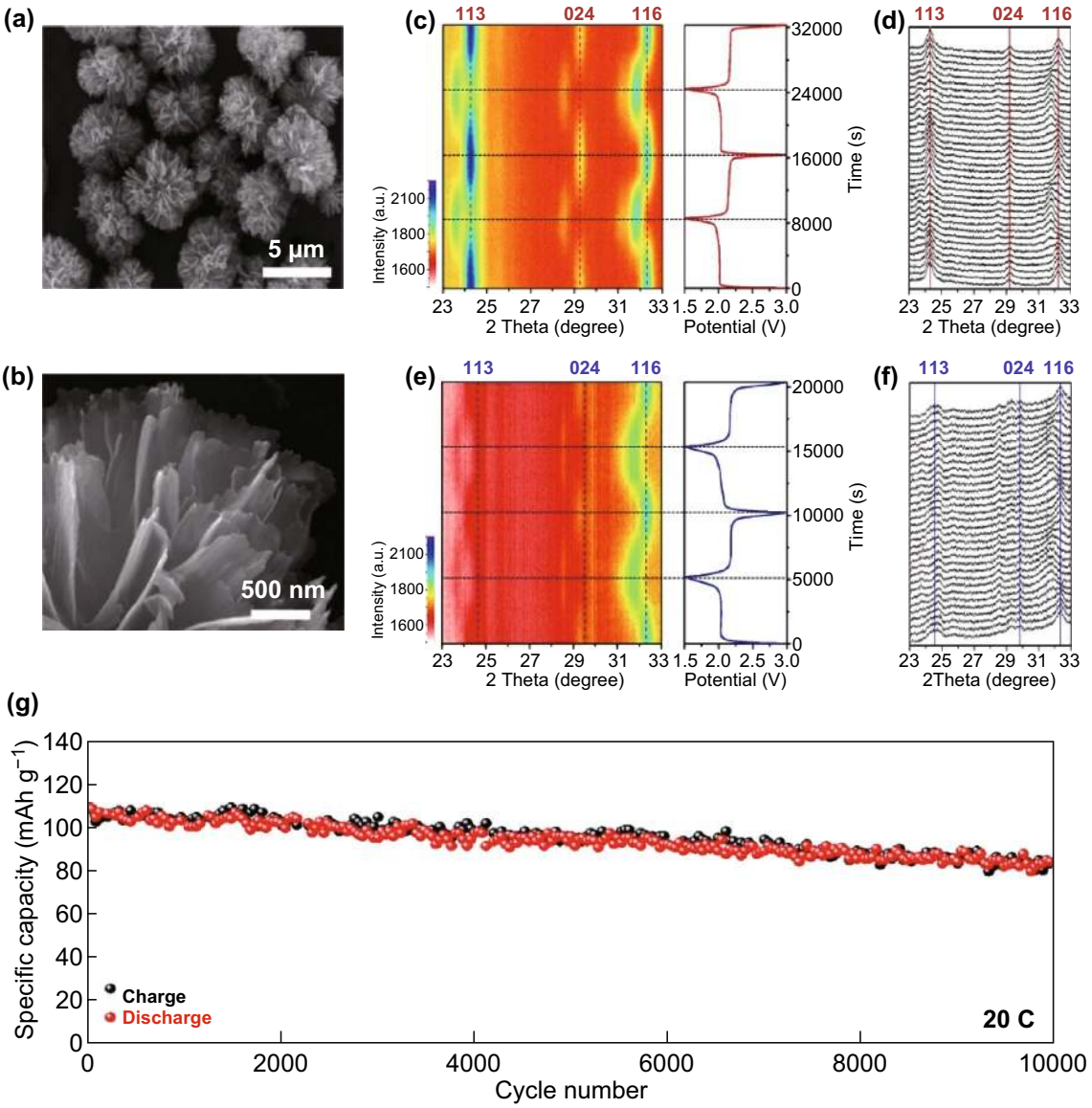

Fig. 4 **a**, **b** Field emission SEM images of carbon-coated hierarchical $NaTi_2(PO_4)_3$ mesoporous microflowers (NTP/C-F), and in situ XRD patterns of the carbon-coated NTP particles (NTP/C-F and NTP/C-P)) half-cells during galvanostatic discharge and charge at 50 mA g^{-1} and a voltage range of 1.5–3.0 V. **c** image plot of diffraction patterns and **d** selected individual diffraction patterns of the NTP/C-F stacked against the voltage profile at 23–33° during the first two discharge–charge cycles. **e** Image plot of diffraction patterns and **f** selected individual diffraction patterns of the NTP/C-P stacked against the voltage profile at 23–33° during the first two discharge–charge cycles. **g** Ultralong cycling stability of the NTP/C-F for 10,000 cycles at 20 C [41]. Copyright 2016, Elsevier Ltd

reversible structure change during sodiation/desodiation. The superior performance can be ascribed to the synergistic effect of the carbon skeleton for structural stability, as well as to the highly stable and open framework with rich mesopores for intimate contact between the electrolyte and active nanosized NTP of rapid Na-ion diffusion and electron transport [41].

Apart from carbon, TiO_2 has also proved to be an efficient coating layer for NTP. Yang et al. [84] designed a type of highly regular and single-crystalline NTP nanocubes (average diameter ca. 500 nm) with a synergistic nanocoating of carbon and rutile TiO_2 (C/NTP-RT) (Fig. 5a, b). The amorphous carbon layer (thickness ~ 10 nm and carbon content of ~ 4.2 wt%) was coated on NTP-RT to enhance the electronic conductivity for higher rate capability. When applied to an SIB anode, the C/NTP-RT exhibited capacitor-like superb rate performance and battery-like high capacity and ultralong-life feature; e.g., over 10,000 cycles, it could deliver a high rate capacity of 72.3 mAh g^{-1} with a capacity retention of 89.3% (of the initial 83.5 mAh g^{-1}) at 10 C (Fig. 5c). This facile one-step hydrothermal method of TiO_2 precursor addition provides a new strategy for optimizing electrode materials and may be utilized in future high-rate, ultra-stable, and low-cost energy storage applications.

Embedding the NTP nanoparticles in the nanocarbon networks will considerably enhance the Na-ion/electron transfer for highly reversible and ultrafast sodium storage [79, 85–88]. For example, by using a simple soft-template method, Yu and coworkers designed an NTP/C composite with nanosized NTP particles coated by a thinner carbon shell and interconnected by a carbon network. With the synergistic effects of a lower charge transfer resistance and a larger surface area for the electrolyte to soak in and sufficient void to buffer the volume variation during the repeated Na^+ insertion/extraction, the anode materials demonstrated outstanding rate performance (108 mAh g^{-1} at 100 C; i.e., a discharge/charge time of 36 s) and long cycle life (83 mAh g^{-1} at 50 C over 6000 cycles), as well as a lower polarization and higher initial CE (ICE; e.g., ~ 98% at 1 C) [85]. Similar to amorphous carbon networks, carbon nanotubes are also a superior framework for enhancing Na^+/e^- conductivity. Xu et al. fabricated a hierarchical porous nanocomposite architecture consisting of MWCNT-threaded mesoporous NTP nanocrystals for high-performance sodium electrodes. With a high ICE of 99%, high rate capability of 74 mAh g^{-1} at 50 C, and long-term cycling stability (74 mAh g^{-1} after 2000 cycles at 10 C) superior to that of the physically mixed reference composite, it provides a general hetero-assembly approach to various types of nanocomposites for high-performance SIBs [79]. Wang et al. [86] designed a carbon-nanotube-decorated NTP/C nanocomposite with high rate performance; especially impressive is that the composite could exhibit low-temperature (− 20 °C) performance with a capacity of 65 mAh g^{-1} at 10 C. Wei et al. fabricated porous $NaTi_2(PO_4)_3$/C hierarchical nanofibers (Fig. 5d, e) via an electrospinning method followed by annealing. The NTP/CNFs as an anode for SIBs exhibited a high reversible capacity of 120 mAh g^{-1} at 0.2 C, high rate capability (71 mAh g^{-1} at 20 C), and long cycling stability similar to those of sodium-ion full cells and hybrid sodium-ion capacitors. When assembled using nickel hexacyanoferrate (NiHCF, $Na_4Fe(CN)_6$) as cathode material, it showed a high ICE of ~ 90% (corresponding to initial charge and discharge capacities of approximately 122 and 110 mAh g^{-1}) and a capacity retention of ~ 90% after 500 cycles at 150 mA g^{-1} with a CE that approached 100% as well as excellent rate capabilities when operated between 0.5 and 2.5 V (Fig. 5f, g) [75]. Yu et al. prepared a similar structure of ultrafine nanoparticles encapsulated in 1D N-doped carbon nanofibers and extended the voltage window to 0–3.0 V. The poor electrical conductivity of NTP was significantly improved, and the composite demonstrated stable and ultrafast Na storage capability with a specific capacity of 121 mAh g^{-1} at 10 C after 2000 cycles and 105 mAh g^{-1} after 20,000 cycles, as well as superior rate performance from 0.2 to 20 C with a recovery efficiency of 99.4% [76].

Full cell batteries with high energy and long life cycle remain a significant challenge, and the formation of an SEI on both cathodes and anodes (especially for the hard-carbon-incorporated composites) has revealed a potential way to realize long-term stability of SIB full cells. A pre-cycling of cathodes and anodes leads to pre-formation of an SEI, which mitigates the additional consumption of Na^+ ions in full cells for higher ICE as well [89–94]. In addition, the adoption of Al (compared to the more common choice, Cu) as the anode current collector in NASICON NTP//NVP full cells will enhance the specific energy, although some improvements are needed to achieve better power capability and energy efficiency [95]. The simultaneous optimization of the structural stability of cathode materials will further enhance the cycle performance of the Na-ion full cells [96].

https://doi.org/10.1007/s40820-019-0273-1

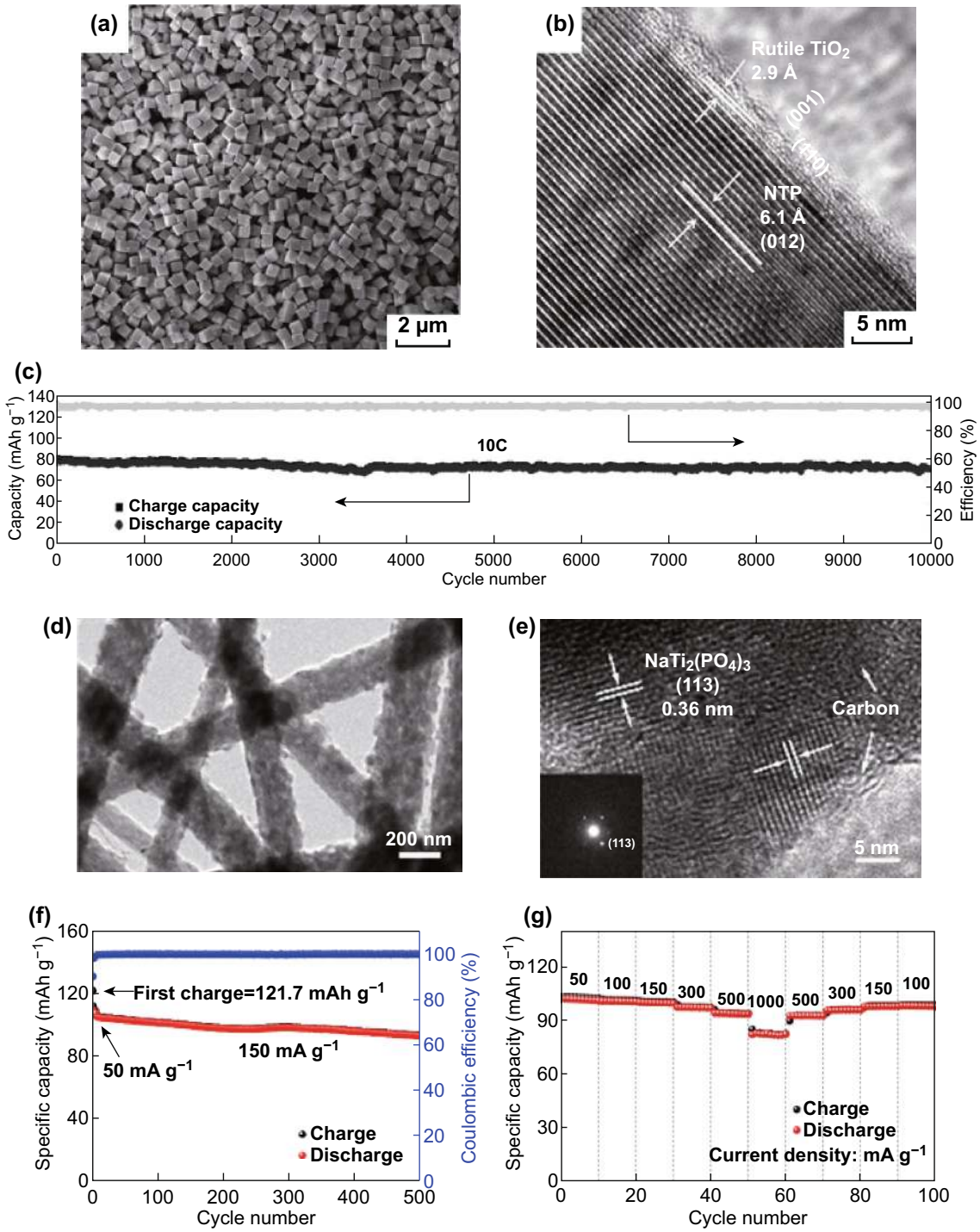

Fig. 5 **a** SEM image and **b** HRTEM image of NTP-RT at the edge and **c** ultralong-term cycling performance at a high current density of 10 C [84]. Copyright 2015, Wiley–VCH Verlag. **d, e** TEM images at different magnifications. **f** Cycling stability and **g** various charge/discharge rates of NTP/CNFs//NiHCF full cell [75]. Copyright 2018, American Chemical Society

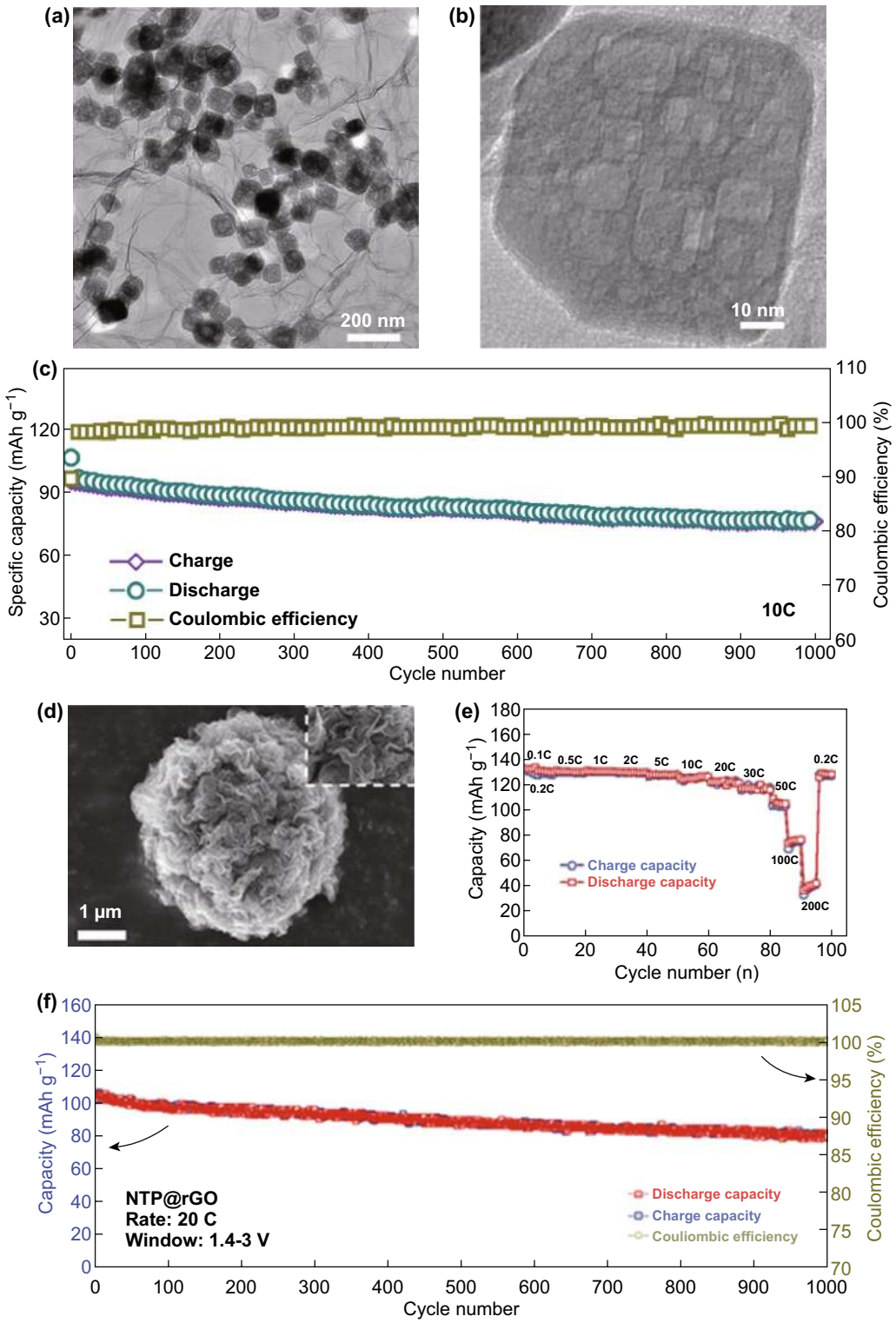

Fig. 6 **a** TEM and **b** HRTEM images of NTP⊂GN and **c** long cycling performance of the NTP⊂GN electrodes. Note that all the capacity values for the NTP⊂GN electrodes are calculated on the basis of the mass of NTP, which is 65% of the whole electrodes including NTP, graphene, carbon black, and PVDF [45]. Copyright 2015, American Chemical Society. **d** SEM images showing a 3D graphene network obtained by removing $NaTi_2(PO_4)_3$ nanoparticles with HF solution. **e** Rate capability of the NTP@rGO electrode. **f** Long-term cycling performance of the NTP@rGO electrode at a high current rate of 20 C over 1000 cycles in the voltage window 1.4–3.0 V [44]. Copyright 2016, Wiley–VCH

https://doi.org/10.1007/s40820-019-0273-1

2.1.3 2D NTP Composites

Two-dimensional (2D) graphene and its analogs are an ideal conductive matrix for electrochemical applications owing to its excellent electrical conductivity, high specific surface area, and mechanical robustness [27, 63, 97–101]. The Yu group synthesized a novel architecture of porous NTP nanoparticles embedded in 3D graphene networks (NTP⊂GN) (Fig. 6a, b) via a self-assembly and post-heat-treatment route. By synergistically combining the advantages of a 3D graphene network and 0D porous nanoparticles, the architecture significantly facilitates the electron/ion transport kinetics and ensures electrode structure integrity, leading to excellent electrochemical performance as reflected by the high rate capability (112, 105, 96, 67 mAh g^{-1} at 1, 5, 10, 50 C, respectively), long cycle life (80% capacity retention over 1000 cycles at 10 C), and a high ICE (> 79%) (Fig. 6c). The ultrafast and stable performance as a promising advanced SIB anode exceeds that of other hard carbon or metal alloy materials, and is comparable to that of supercapacitors [45].

Fang et al. designed 3D-graphene-decorated $NaTi_2(PO_4)_3$ microspheres (NTP@rGO) (Fig. 6d) via a hierarchical graphene-embedded process using a facile spray-drying method with post-calcination for superior high rate and ultracycle-stable sodium storage performance as a promising SIB anode [44]. The as-obtained NTP@rGO composite demonstrated a high reversible capacity of 130 mAh g^{-1} (close to 96% theoretical capacity) at 0.1 C (with almost equal values from 0.1 to 2 C; 1 C = 133 mA g^{-1}), long stable cyclability (77% capacity retention over 1000 cycles at 20 C), and ultrahigh rate capability (38 mAh g^{-1} at 200 C) (Fig. 6e, f). When paired with $Na_3V_2(PO_4)_3$ as a cathode, the NTP@rGO//NVP/C full cell can deliver a high discharge capacity of 128 mAh g^{-1} at 0.1 C based on the anode mass, and an outstanding long-life cycling performance with 80% capacity retention over 1000 cycles and a CE of above 99.5%, as well as a high rate performance of 88 mAh g^{-1} at 50 C. The SIB full cell exhibited excellent specific energy and power densities that are superior to those of hybrid batteries and supercapacitors [102, 103], showing an energy density of 73 Wh kg^{-1} at a power density of 7.6 W kg^{-1} (0.1 C) and even maintaining 38.6 Wh kg^{-1} at a power density up to 3167 W kg^{-1} (50 C). The excellent properties can be attributed to the combined advantages of the graphene-coated nanosized NTP particles and the presence of the highly conductive 3D graphene network, which remarkably enhanced the ionic/electronic transport and buffered the volume variation during sodiation and desodiation. The novel method for 3D hierarchical spherical structures shows a promising alternative route for realizing superior SIBs.

Some similar structures also showed excellent performance because the nanosized structures and the intimate contact between NTP and high-conductive graphene significantly reduced the transport lengths of the Na^+ ions and the "expressway" of electron transport [61, 104, 105]. For example, a phase-pure $NaTi_2(PO_4)_3$/reduced graphene oxide (rGO) nanocomposite, prepared using a microwave-assisted one-pot solvothermal method and post-heat treatment with well-crystallized and uniformly anchored NTP nanoparticles (30–40 nm) on an rGO matrix through Ti–O–C bonds, can exhibit a high specific capacity of 129 mAh g^{-1} (approaching the theoretical value) at 0.1 C and an excellent rate capacity (72.9% capacity retention at 50 C), as well as superior cycling performance with merely 4.5% capacity loss over 1000 cycles at a high rate of 10 C (the CE remained at 99.8%) without using any other additional conducting agent in the anode. Furthermore, the NTP/rGO nanocomposite showed excellent high-temperature cyclability up to 55 °C [106]. Ma and coworkers designed and developed a structure consisting of porous $NaTi_2(PO_4)_3$ nanocubes (50–100 nm) anchored on porous carbon nanosheets (average thickness of ~ 10 nm) for high rate capability. With the extended potential window of 0.01–3.0 V, the open 3D framework structure exhibited a high initial discharge capacity of 485 mAh g^{-1} at 0.1 A g^{-1}, and a high capacity of 98 mAh g^{-1} was retained at 4.0 A g^{-1} after 2000 cycles [107]. However, the low ICE needs to be improved for further practical application in full SIBs. In addition, by incorporation of 2D MXene nanosheets with inherent advantages including a suitable interlayer spacing for accommodating sodium ions, low working potentials, environmental benignity, and exceptional chemical durability [108–111], Zhi and coworkers designed a dual-mode sodium storage device based on the combination of pseudocapacitance-type and battery-type electrochemical behavior. The dual-mode anode material (MXene@NTP-C) (Fig. 7a, b) for SIBs showed superior rate capacities (208–102 mAh g^{-1} at 0.1–10 A g^{-1} within the voltage window 0.1–3.0 V vs. Na/Na^+) as well as remarkable cycling performance up to 10,000 cycles (109 mAh g^{-1} at 5 A g^{-1}) (Fig. 7c–e), which presents an opportunity to balance the energy and power densities [110].

2.1.4 Flexible or Binder-Free Electrodes

Flexible energy storage devices are attracting considerable interest in next-generation bendable, wearable, or implantable electronic systems [112–118]. The Cao group constructed a flexible and binder-free sandwich-structured $NaTi_2(PO_4)_3$ film electrode (Fig. 8a–d) with a two-step graphene hybridizing method for an ultra-stable and long-life SIB anode. The flexible anode with an interconnected framework exhibited excellent cycling stability for sodium half-cells (91% capacity retention over 1000 cycles at 500 mAh g^{-1}) (Fig. 8e). When assembled into flexible full SIBs with $Na_{0.44}MnO_2$ as a cathode, it showed good cycling performance both under flat and bent states as well as a high

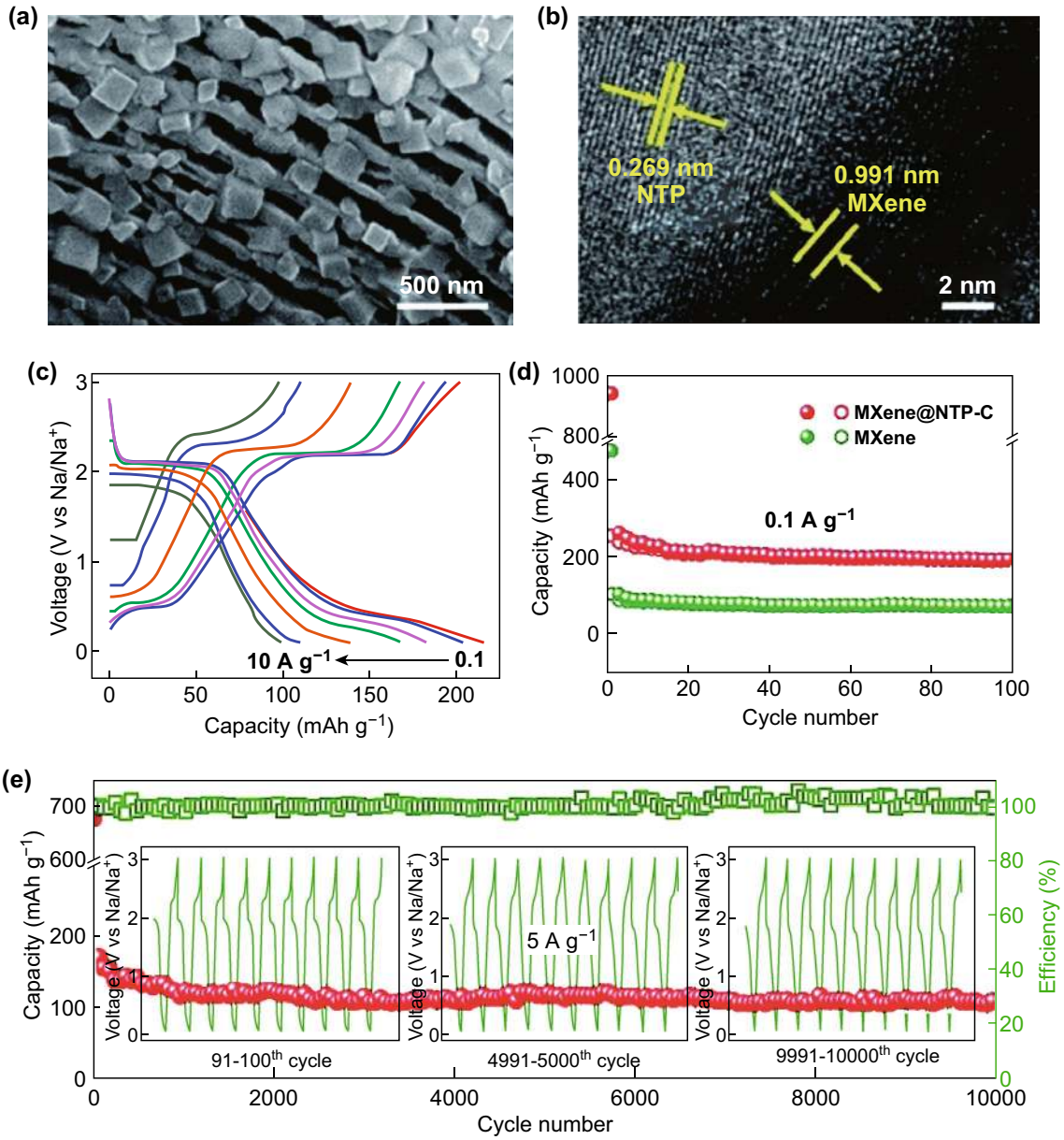

Fig. 7 **a** TEM and **b** high-magnification TEM images of MXene@NTP-C. **c** Galvanostatic discharge/charge profiles of MXene@NTP-C at varied current densities of 0.1–10 A g^{-1}. **d** Cycling performance of MXene@NTP-C and MXene at 0.1 A g^{-1}. **e** Cycling performance of MXene@NTP-C at high current densities of 5 A g^{-1}. The inset of **e** shows the voltage–cycle profile at three different stages [110]. Copyright 2018, the Royal Society of Chemistry

https://doi.org/10.1007/s40820-019-0273-1

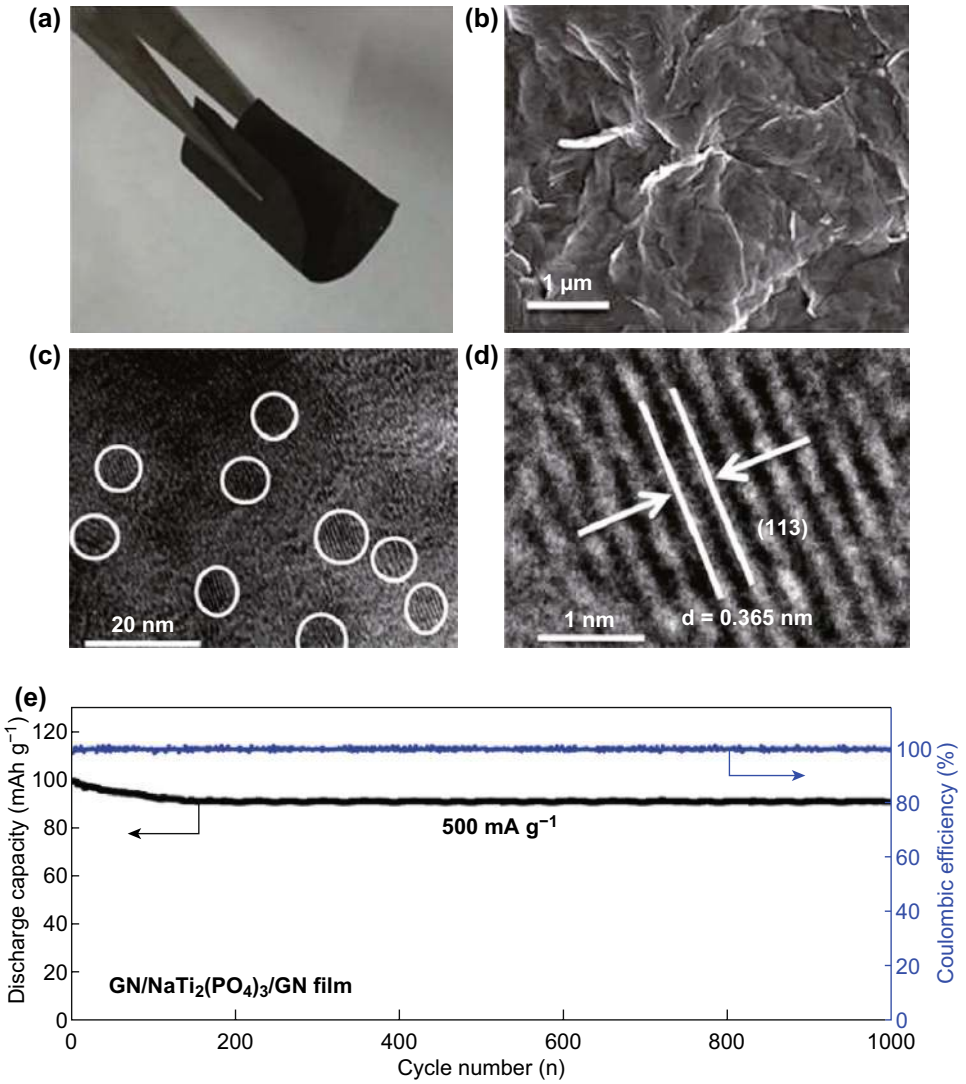

Fig. 8 **a** Digital photograph and **b** FESEM images of the as-fabricated flexible GN/$NaTi_2(PO_4)_3$/GN film. **c, d** HRTEM images of GN/$NaTi_2(PO_4)_3$/GN film. **e** Long-term cycling stability of GN/$NaTi_2(PO_4)_3$/GN film electrode at 500 mA g^{-1} [112]. Copyright 2018, American Chemical Society

ICE (82.3%) in the voltage window 2.0–4.0 V [112]. Previous work has reported the design of a synergistic flexible electrode, mesoporous NTP nanocrystals embedded in monolithic hierarchical porous carbon assembly rGO and CNTs for high-performance SIBs (maintaining a high reversible capacity of 125 mAh g^{-1} at 1 C, long cycling life of 5000 cycles at 10 C with 82% capacity retention, and high rate capability of 73 mAh g^{-1} at 30 C; superior to the rGO-only recipe) [114], as well as other self-supporting anodes such as mesoporous NTP nanocrystals confined in MWCNTs network (film thickness of 50 μm; showing a high volumetric/areal capacity: 132 mAh g^{-1} at 1 C with ICE of 99%, 62 mAh g^{-1} at 50 C, and long-term cycling stability with a capacity of 87% at 10 C after 3000 cycles) [119]. Yang and coworkers constructed another 2D nanocomposite architecture comprising mesoporous NTP nanocrystals, rGO, and thermally treated protein (TP) (denoted by MNTP-TP@rGO) as a free-standing electrode for an advanced SIB anode. The 3D interconnected carbon network of rGO and TP acts as a support for anchoring the well-distributed mesoporous NTP nanocrystals and also a current collector. As a free-standing anode for a half-cell, it delivered a high rate capacity of 52.8 mAh g^{-1} at 50 C and robust cycling stability (80% capacity retention over 1000 cycles at 5 C).

When paired with $Na_3V_2(PO_4)_3$/C (NVP/C) as a cathode, the free-standing anode demonstrated a high specific capacity of 58 mAh g^{-1} with outstanding cycling stability (98% capacity retention over 100 cycles at 1 C) [113]. However, it should be noted that despite a flat voltage plateau, the voltage is only approximately 1.2 V lower than that of the full cell with $Na_{0.44}MnO_2$ as a cathode [112]. The strategy developed here can provide a general route for preparing other graphene-based flexible SIBs.

2.1.5 High-Safety SIBs

Development of high-safety and long-lifespan SIBs is urgently needed for large-scale energy storage applications. All-solid-state SIBs have attracted considerable attention for their safety and long-term durability [120–125]. Solid-state rechargeable SIBs based on ceramic (e.g., Na-β″-Al_2O_3) electrolyte with high sodium ion conductivity can demonstrate an extremely stable voltage plateau of ~ 2.1 V in the half-cell and an initial discharge capacity of 133 mAh g^{-1}, although the cycling and rate performances may be improved via modification of interfacial incompatibility (or cell resistance and intrinsic polarization) compared to that of typical non-aqueous SIBs [126]. To further suppress the formation of Na dendrite, Goodenough and coworkers designed a NASICON ceramic electrolyte assisted by an in situ-formed thin interfacial interlayer or by the introduction of a dry polymer layer for high-temperature performance and safety advantages. The as-prepared all-state-batteries with NTP as the anode showed high cycling stability and CE (99.8 ± 0.02%) at 65 °C due to the enhanced wetting of sodium on the interfacial interlayer that suppresses dendrite formation and growth.

Currently, most batteries for electrical energy storage (EES) use highly flammable and volatile organic carbonate esters as electrolytes, which may cause severe safety problems, and an intrinsic system is in high demand, especially for large-scale EES applications [127]. Apart from aqueous electrolytes [128] and solid-state electrolytes, etc., [121, 126, 129], proton-type organic phosphonates have demonstrated promise for safer SIBs with a wide electrochemical window and high ionic conductivity [127, 130]. Cao and coworkers designed and constructed an interesting all-phosphate-based battery by using a NTP anode, $Na_3V_2(PO_4)_3$ cathode, and trimethyl phosphate (TMP) electrolyte for zero-strain SIBs with intrinsic safety, high rate performance, and long cycle life [127]. The full cells demonstrated good cycling performance (73.7% capacity retention over 1000 cycles) and promising designing flexibility for practical application. Soon after that, a similar self-standing all-phosphate SIB with high mass loading for fast cycling was realized [131].

For large-scale and low-cost energy storage, non-aqueous semi-solid flow batteries (SSFBs)—a special class of redox flow batteries (RFBs)—based on the rich chemistry of Na-ion intercalating compounds, e.g., the NTP anode and P2-type cathodes, may serve as an inspiration [132].

2.1.6 Trace-Element-Doped NTP Materials

As an effective method of improving the electrochemical performance of electrode materials, lattice doping has been proposed and widely used in LIBs and SIBs [133]. As for research on NTP-based materials, it was first demonstrated by Mouahid and coworkers [134] that the doping of Al is beneficial for improving the ionic conductivity of NTP and improves electrochemical performance. Tirado's group proposed that the low content of iron doping did not change the lattice structure but could enhance the capacity values and improve capacity retention [135–137]. Goodenough's group utilized the NASICON-structured $Na_3MnTi(PO_4)_3$ as both the anode and cathode to construct an aqueous symmetric SIB with an operating voltage of 1.4 V, stable cycle performance, and excellent rate capability [138]. Dai's group demonstrated that Sn doping on the Ti site shows no obvious effect on the lattice structure and morphology of $NaTi_2(PO_4)_3$/C but is very beneficial for improving the electrochemical properties of the $NaTi_2(PO_4)_3$/C anode for aqueous LIBs [139]. Zhang and coworkers reported the synthesis of porous $Na_3MgTi(PO_4)_3$ aggregates with a sol–gel method. The good rechargeable capacity of 54 mAh g^{-1} and better capacity retention performance (94.2% after 100 cycles) of $Na_3MgTi(PO_4)_3$ compared to those of NTP demonstrate that the incorporation of electrochemically inert Mg^{2+} ions could improve the structural stability of Na storage materials and enhance cycling performance [140].

2.2 Aqueous Batteries

Aqueous rechargeable alkali-ion (e.g., Li, Na, Mg-ion) batteries that do not employ costly, highly toxic, and flammable

 https://doi.org/10.1007/s40820-019-0273-1

organic solvents were first reported by Dahn's group in 1994 using $VO_2/LiMn_2O_4$ electrodes and $LiNO_3$ aqueous solution as the electrolyte. Because of the much higher ionic conductivity of the aqueous electrolyte compared to that of organic electrolytes, aqueous batteries always feature high round-trip efficiency and energy density and have attracted interest as possible substitutes for conventional non-aqueous rechargeable systems. However, the narrower stable voltage window and the poor cycling life of aqueous electrolytes compared with those of organic electrolytes prompted researchers to further develop high-performance aqueous rechargeable alkali-ion batteries [43, 141, 142]. Of equal or greater interest, due to the high natural abundance of sodium, low lost, and safety advantages for large-scale or stationary energy storage, are aqueous sodium-ion batteries (ASIBs) or aqueous rechargeable sodium batteries (ARSB) [19, 43, 128, 143–145]. Okada and coworkers first presented a working demonstration of the aqueous Na-ion full cell using an NTP anode [43, 47] and revealed that an aqueous electrolyte showed a higher conductivity and lower viscosity compared with those of non-aqueous (i.e., organic) electrolytes, as well as much smaller interfacial activation energy or higher kinetics of Na-ion transfer than those of Li-ion secondary batteries, which are advantages for high rate capabilities [47, 57, 146, 147].

However, NTP suffers from considerable capacity fade when cycled slowly and deeply, and this could be attributed to the increasing pH caused by the presence of OH^- ions when water was reduced by Ti(III) ions at the surface of the electrode material and the following alkaline oxidation of the carbon conductive additive to carbonate ions at potentials lower than − 1.38 V versus Hg/Hg_2SO_4, which finally causes loss of electrical contact and ultimately failure of the cell [148]. Some studies reveal that the formation of amorphous transition metal phosphate layers and/or insoluble titanium sulfate phases on the surface of NTP particles, which are ionically and electronically insulating, via dissolution of sodium and titanium cations and hydrolysis of surface groups, may block the electrolyte access pathways to the electroactive particles embedded in the electrode and lead to capacity fade, although a deeper understanding of ''phosphate–aqueous solution interface'' reactions requires further investigations [149]. Upon optimizing the design and synthesis of nanostructured and higher conducting NTP composite anodes (e.g., NTP/C [60, 62, 150–152], NTP@C/Ag [153], NTP/conducting-polymers [148], or doped NTP [154]), the Na-ion diffusivity and electronic conductivity limitations encountered can be removed as well in organic electrolyte systems [43]. These composite structures include a self-assembled hierarchical carbon-decorated wafer-like 3D porous NTP/C composite with bicontinuous electron transport pathways via a surface nanoscale carbon layer and a porous microscale carbon matrix over NTP particles (Fig. 9a–d) (rate capability of 63 mAh g^{-1} high up to 50 C, and a stable capacity of 92 mAh g^{-1} over 300 cycles at 2 C with CE nearly 100%) [155]; a frogspawn-inspired hierarchical NTP/C (core–shell) array (rate capability of 78 mAh g^{-1} at 60 C, capacity retention of 88% at 1 C over 400 cycles and 89% at 20 C over 2000 cycles with a CE of nearly 100%) [156]; an NTP/C composite synthesized by a modified Pechini method and pyrolysis treatment, delivering an initial capacity of 129 mAh g^{-1} and maintaining 117 mAh g^{-1} over 50 cycles at 2 C and a high rate capability of 66 mAh g^{-1} at 20 C [150]; an NTP/CNTs/graphite composite in situ-synthesized with intermixed "intimate carbons", showing improved performance (82 mAh g^{-1} over 100 cycles at 1 C with CE > 99.7%) over that with post-synthesized or with individual carbon [157]; and other composites with commercial carbon black or graphite [151].

Generally, the incorporation of 3D-carbon-based porous frameworks with high conductivity, high surface area, high structural stability, and good electrolyte penetration has attracted particular attention and exhibited high-efficiency electro/ion transport and better performance, and is thus considered an effective strategy for fabricating high-performance ASIBs [155]. Graphene, as a new and ideal 2D carbon material, has attracted intensive attention for application in energy conversion and storage due to its superior electrical conductivity, high surface area, structural flexibility, etc. The incorporation of graphene to form NTP composites or hybrids as a highly electronically conductive network improved cycling stability and rate performance, as was recently reported [59, 97]. For example, Zhang and coworkers prepared a 2D hybrid nanoarchitecture of NTP/graphene with highly crystalline NTP nanoparticles homogeneously anchored on the surface of conducting graphene nanosheets via a solvothermal method followed by calcination. The nanocomposite (with only 3.4 wt% of graphene) used as anode materials for ASIBs exhibited excellent electrochemical performance with high rate capabilities (110, 85, 65, and 40 mAh g^{-1} at 2, 5, 10, and 20 C, respectively) and a good cycling stability with 90% retention of the initial

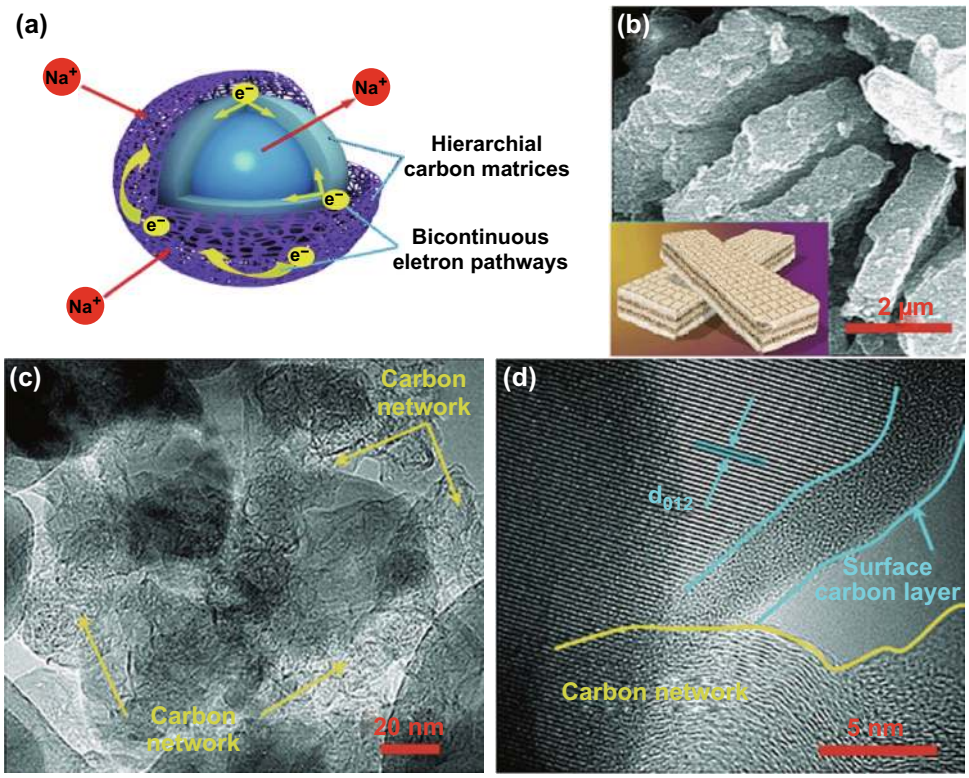

Fig. 9 **a** Schematic image of enlarged parts in the wafer-like architecture with bicontinuous pathways for high-efficiency electron/ion transport. **b** SEM images of the wafer-like particles. **c** TEM image of the wafer-like particle. **d** HRTEM image of one primary particle decorated by hierarchical carbon [155]. Copyright 2015, the Royal Society of Chemistry

capacity over 100 cycles at 2 C. The remarkable improvement in specific capacity, rate performance, and cycling stability can be ascribed to the unique structures and the merits of both ingredients [59].

Apart from carbon components, a TiN layer was also applied on the surface of NTP to enhance the electronic conductivity in an aqueous electrolyte system. Zhang and coworkers synthesized a TiN-coated $NaTi_2(PO_4)_3$ as an anode material for aqueous SIBs via a solvothermal routine and a subsequent nitriding process (i.e., calcination in ammonia gas). The optimized TiN-tailored NTP particles showed an improved rate capability and cycling performance with an initial capacity of 132 mAh g^{-1} and maintained 92 mAh g^{-1} after 100 cycles at 2 C, a large improvement over the pristine phase [158].

2.2.1 Full Cells

When combining with the cathodes, e.g., layered $NaMnO_2$ [159], Na-birnessite with crystal water [160], alkali-cation-incorporated δ-MnO_2 [161–163], Prussian-blue-type $Na_2CuFe(CN)_6$ [164], $Na_2NiFe(CN)_6$ [46], tunnel-structured $Na_{0.44}MnO_2$ ($Na_4Mn_9O_{18}$) [43, 80, 152, 165, 166], NASICON-structured $Na_3V_2(PO_4)_3$ [167], and $Na_2VTi(PO_4)_3$ [168], the aqueous SIBs exhibited high energy density and good cycle stability, which are particularly attractive for stationary energy storage applications. The use of Na-deficient NTP as an anode and Na-rich cathodes in an aqueous electrolyte system may be visually depicted as a "rocking-chair-type" SIBs [46]. In the full cells of an NTP system, it is generally agreed that the low electronic conductivity of the NTP anode was rate limiting, and by eliminating this limitation via NTP/C composite optimization, for example, ultrafast rate capability and superior high rate cycling stability can be obtained [80, 157, 165]. Chiang and coworkers demonstrated an ultrafast rate (> 100 C) and superior high rate cycling (> 1500 cycles) for aqueous $NaTi_2(PO_4)_3/Na_{0.44}MnO_2$ (NTP/NMO) cells with a specific volumetric energy density of up to 127 Wh L^{-1} from the materials-only level, and a cell level density

 https://doi.org/10.1007/s40820-019-0273-1

of ~ 65 Wh L^{-1} may be expected, which exceeds the energy density of more fully developed active carbon (AC)/NMO systems. The NTP–C nanocomposite synthesized by ball milling a 2–3% pyrolytic carbon from the glucose precursor accounts for the superior performance [43]. Zhang and coworkers further studied an NTP/MWCNTs–$Na_{0.44}MnO_2$ system to improve the electronic conductivity [165]. Thus, aqueous NTP/NMO may become a candidate for safe, low-cost, and high-power storage systems. However, possible causes for low-rate capacity fade may recur due to some complicated side reactions, e.g., partial diffusion of electrode materials, oxidation of the anode in its sodium-inserted state by dissolved oxygen or oxygen generated via water hydrolysis, or oxidation of the aqueous electrolyte by the charged cathode [43, 47]. For flexible aqueous SIBs, Guo et al. designed and fabricated a family of safe flexible SIBs as potential wearable or even implantable electronic devices based on a nanosized $NaTi_2(PO_4)_3$@C anode, a $Na_{0.44}MnO_2$ cathode, and various Na^+-containing aqueous electrolytes (including Na_2SO_4 solution, normal saline, or cell-culture medium), compared to that of either toxic flammable organic solutions or strong acid/base as electrolytes. The as-prepared belt- and fiber-shaped ASIBs exhibited excellent electrochemical performance (with high volumetric energy and power density, and long life) as well as high flexibility. This fiber-shaped electrode system also exhibited electrochemical deoxygenation and pH-changing features, which might be further applied in biological and medical fields [117].

Cathodes with different potential plateaus often influence the output voltage of the ASIB system [169]. For example, the Prussian-blue-type $Na_2NiFe(CN)_6$ combined with an NTP anode can deliver an average output voltage of 1.27 V, as well as an energy density of 42.5 Wh kg^{-1} and a capacity retention of 88% over 250 cycles at a 5 C rate [46]. Furthermore, adjustment of the transition metal cations at the M site in the Prussian blue compounds $Na_xM_yFe(CN)_6$ enabled the $Na_2CuFe(CN)_6$ cathode in the same ASIB system to exhibit a higher output voltage of 1.4 V (with a well-defined discharge plateau and a slight decrease from 1.4 to 1.1 V) as well as an enhanced energy density (48 Wh kg^{-1}), rate, and cycling performance [164]. The NASICON-type $Na_3V_2(PO_4)_3$ assembled aqueous full cell with NTP as the anode demonstrated a flat discharge plateau at 1.2 V and could maintain a high rate performance (58 mAh g^{-1} at 10 A g^{-1}) well, showing a high energy density of 29 Wh kg^{-1} at a power density of 5145 W kg^{-1} [167]. Layered $NaMnO_2$ and its full cells with an NTP anode delivered an inclined curve of the voltage profile (e.g., 1.8–0.5 V) without plateaus, as well as an energy density of 30 Wh kg^{-1} at a power density of 50 W kg^{-1} and could retain 75% of the initial capacity over 500 cycles at 5 C [159]. The tunnel-structured $Na_{0.44}MnO_2$ full cell coupled with NTP showed a distinct flat plateau and an average operation voltage of 1.13 V, slightly lower than that of a typical commercial battery such as the Ni–Cd battery (1.2 V), but an initial reversible specific capacity of 85 mAh g^{-1} [80] or a higher capacity of 114 mAh g^{-1} [155] could be obtained. Through further modification, the Ti-substituted $Na_{0.44}MnO_2$ full cell coupled with an NTP anode could exhibit an average operating voltage of 1.2 V, higher rate capabilities (54 mAh g^{-1} at 10 C), and much more stable cycling performance (76 mAh g^{-1} at 2 C with a very small capacity decay up to 300 cycles) for practical applications [166].

2.3 Electrolyte Dependence of Performance

Various electrolytes have currently been used and developed for non-aqueous SIBs based on the rationale for specific choices regarding cell setup and usage conditions [129]. In regard to aqueous electrolytes, some studies reveal that the full cell with Na_2SO_4 as electrolyte may show poor cyclability and $NaCH_3COONa$ (NaAc) electrolyte exhibits improved performance, for the $NaMnO_2$ cathode suffered from dissolving excessively in the Na_2SO_4 electrolyte followed by rapid capacity loss of the full cell [159]. Although $NaClO_4$ electrolyte showed even a little better performance than that of the Na_2SO_4 electrode, its explosiveness and oxidizing abilities may be concerns in the market [147]. In aqueous $NaNO_3$ electrolyte, the NTP anode exhibits higher intercalation/deintercalation kinetics and reactions that are approximately twice as fast as in $LiNO_3$ solution [57]; further, the NTP anode in Li^+ ion aqueous electrolyte (1 M Li_2SO_4 solution) will suffer from a higher potential plateau together with a suppressed rate performance due to the thermodynamic limitations of the lithium insertion into the Na-containing structure and/or Na^+–Li^+ repulsive interactions [70]. Another study showed that the full cell ($Na_2FeP_2O_7$// NTP) with a higher $NaNO_3$ concentration exhibited a large irreversible capacity due to H_2 gas evolution and corrosive side reactions [147]. NaOH aqueous electrolyte, however, showed poor performance in cycling stability, which may

be due to the decreased stability of the electrode material at higher pH [47, 97, 141].

In aqueous electrolyte SIBs, the salt concentration of the electrolyte affects the ionic conductivity and the rate performance of batteries as well as the diffusion of the reactive species, which can cause self-discharge, particularly in high-mass-loading electrodes. Studies showed that with higher-molarity solutions of typical electrolytes, rate capability and electrode utilization increased significantly (the redox peaks are sharper and closer, which indicates faster kinetics, consistent with the ionic conductivity difference); e.g., by increasing the salt ($NaClO_4$) concentration from 1 to 5 M, the capacity at 1.5 C increased by 38%, and the oxygen-related self-discharge phenomenon diminished, although measurable irreversible capacity loss still occurred with the lowest oxygen content, suggesting that self-discharge and capacity loss are not necessarily causally related [170]. Furthermore, the increase in electrolyte concentration extended the electrochemical window of ASIBs up to 2.8 V (with concentrated 17 mol kg^{-1} $NaClO_4$ aqueous electrolyte compared to the value of only 1.9 V with diluted 1 mol kg^{-1}, which widened the theoretical voltage restriction of 1.23 V due to practical overvoltage) and could produce a higher discharge plateau of 1.8 V in a full cell with the Prussian-blue-type cathode. Higher concentrations of electrolyte under a higher rate condition benefits the more stable performance in ASIB systems due to the reduced water content of the NTP anode and elution of the cathode by alkalization of the aqueous electrolyte [171]. For an extremely high concentration, superconcentrated "water-in-salt" electrolytes (WiSEs) with the decreased activity of water resulting from its coordination with concentrated salt ions (or much more intense cation–anion interaction and pronounced ion aggregation in Na-ion electrolytes revealed by Raman spectra together with molecular-scale simulations) can even noticeably suppress the electrochemical decomposition of aqueous electrolytes (yet a dense, stable, and repairable SEI simultaneously formed) and significantly enhance the long-term cycling stability (e.g., > 1200 cycles at 1 C with negligible capacity losses—0.006% per cycle; and showing an extraordinarily high CE > 99.2% at 0.2 C over 350 cycles) at both low and high rates [172, 173]. However, it needs to be mentioned that highly concentrated electrolyte can potentially raise challenging issues such as corrosion, especially at extreme electrochemical potentials [147, 170], and therefore there should be a balance between the electrolyte concentration and high performance. In addition, aqueous electrolytes with more extreme pH (i.e., pH > 13) or those exposed to higher temperatures (e.g., 70 °C) will induce significant structural degradation and precipitation of a secondary phase (i.e., via loss of phosphate to layered sodium titanate) [174]. An aqueous/non-aqueous hybrid electrolyte with an expanded electrochemical window of up to 2.8 V and high conductivity was also explored, which inherited the safety feature of aqueous electrolytes and the electrochemical stability of non-aqueous systems [175].

Although the neutral pH aqueous electrolyte SIBs with clean, non-flammable, fast internal ion transportation, and relatively lower manufacturing cost have shown considerable advantages, especially for large-scale energy storage applications (i.e., promising solutions for applications where constraints on energy density and weight are less rigid) compared with SIBs based on organic electrolytes, the stability window of water limits the voltage of an aqueous cell. Fortunately, researchers have found some solutions that enable the practical stability window of aqueous electrolytes to be widened beyond the theoretical limit via the kinetic effect, which enables the usage of materials whose operating potential exceeds the thermodynamic limit of pure water in an aqueous system [170, 176]. Despite the low cost and eco-friendly features of ASIBs that make them promising candidates for future energy storage systems, aqueous batteries are very much constrained by electrolyte degradation. Electrolyte additives (e.g., vinylene carbonate or other low-cost acetic additives) can further enhance the cycle stability of the full cell [177]. Date from the large-format energy storage device showed promising commercial application of ASIBs of cycle-stable high-voltage strings of cells (Fig. 10a–g) [176].

All-solid-state SIBs have attracted considerable attention for their safety and long-term durability [122–125]. Apart from the typical SIBs based on liquid electrolytes, solid-state rechargeable SIBs based on ceramic (e.g., Na-β″-Al_2O_3) electrolyte with high sodium-ion conductivity can demonstrate an extremely stable voltage plateau of ~ 2.1 V in the half-cell and an initial discharge capacity of 133 mAh g^{-1}, although the cycling and rate performances may be improved via modification of interfacial incompatibility (or cell resistance and intrinsic polarization) compared to that of typical non-aqueous SIBs [126].

Aqueous rechargeable batteries (ARBs), or hybrid aqueous batteries (HABs), based on the migration of two or more types of shuttle ions, will not only enrich

 https://doi.org/10.1007/s40820-019-0273-1

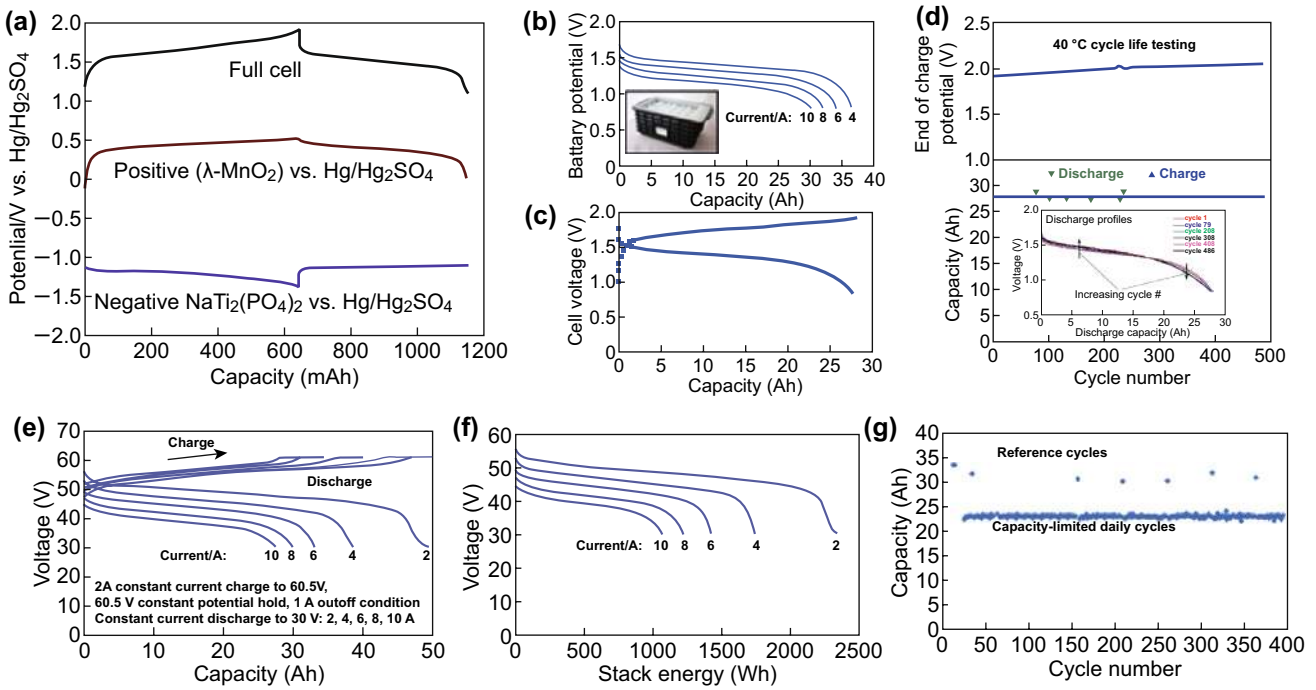

Fig. 10 **a** Three electrode potential-limited constant-current charge/discharge data of a full cell containing the λ-MnO_2 positive electrode and NTP negative electrode, showing the relative potential of the active materials during use. Cycle life data (**b**–**d**) (voltage profile shown in **b**; ±4 A constant-current charge and discharge, with a capacity-limited charge and a voltage-limited discharge) from a large-format unit with 28 Ah capacity. These data were collected at a constant temperature of 40 °C, and this test is ongoing (nearly 800 cycles logged at this point). The maximum voltage reached upon full charge is just above 2 V under 4 A current, which is less than 1.8 V after IR correction. The test is ongoing and has been under way for 14 months. **e**, **f** Performance data for an eight-battery stack showing the delivered energy as a function of current as well as the long-term stability of the battery **g** [176]. Copyright 2014, Wiley–VCH Verlag

the battery families but will also make an operation voltage higher than 1.2 V more available for ARBs [176, 178–192]. For example, NTP–C//LMO ($LiMn_2O_4$) full cells with Li^+/Na^+-mixed electrolyte exhibited enhanced electrochemical performance and anode-dependent electrochemical behavior [178]. For the Li^+/Na^+-mixed electrolyte, both NTP and its counterpart, $LiTi_2(PO_4)_3$, exhibited better rate performance due to the lower diffusion barrier in the NASICON structure compared to that of an electrolyte consisting of single Li^+ ions; the Li or Na ions in the M1 sites of the NASICON materials will be replaced by the ions from the electrolytes with top priority for Na ions [70]. For HABs consisting of electrode materials with selective cation channels, the electrode applicability could increase and thus broaden the application of ARBs. Liu et al. constructed a high-voltage K-Na HAB based on a carbon-coated NTP (open holey nanocube structure) anode and a $K_2FeFe(CN)$ cathode to combine the respective advantages of each material and improve the rate performance and CE (Fig. 11a). Due to the unique cation selectivity of both electrode materials and the ultrafast ion conduction of NTP/C, the hybrid battery delivered a superior capacity of 160 mAh g^{-1} at 0.5 C rate (with an operating voltage ranging from 0.5 to 1.9 V and discharging plateaus at approximately 1.72 and 0.98 V), high rate capabilities (with excellent capacity recovery capability), and a record long-term capacity retention of 94.3% over 1000 cycles at even an ultrahigh rate of 60 C (Fig. 11c–f). Meanwhile, a high energy density of 69.6 Wh kg^{-1} calculated on the total mass of active electrode materials could be obtained, which is comparable to or even superior to that of current commercial aqueous batteries (Fig. 11b) [186]. Using this strategy for integrating different electrode materials with unique cation selectivity toward metal ions, a high-voltage rechargeable aqueous battery will be realized with a high capacity, remarkable energy density, and considerable capacity retention at a high rate.

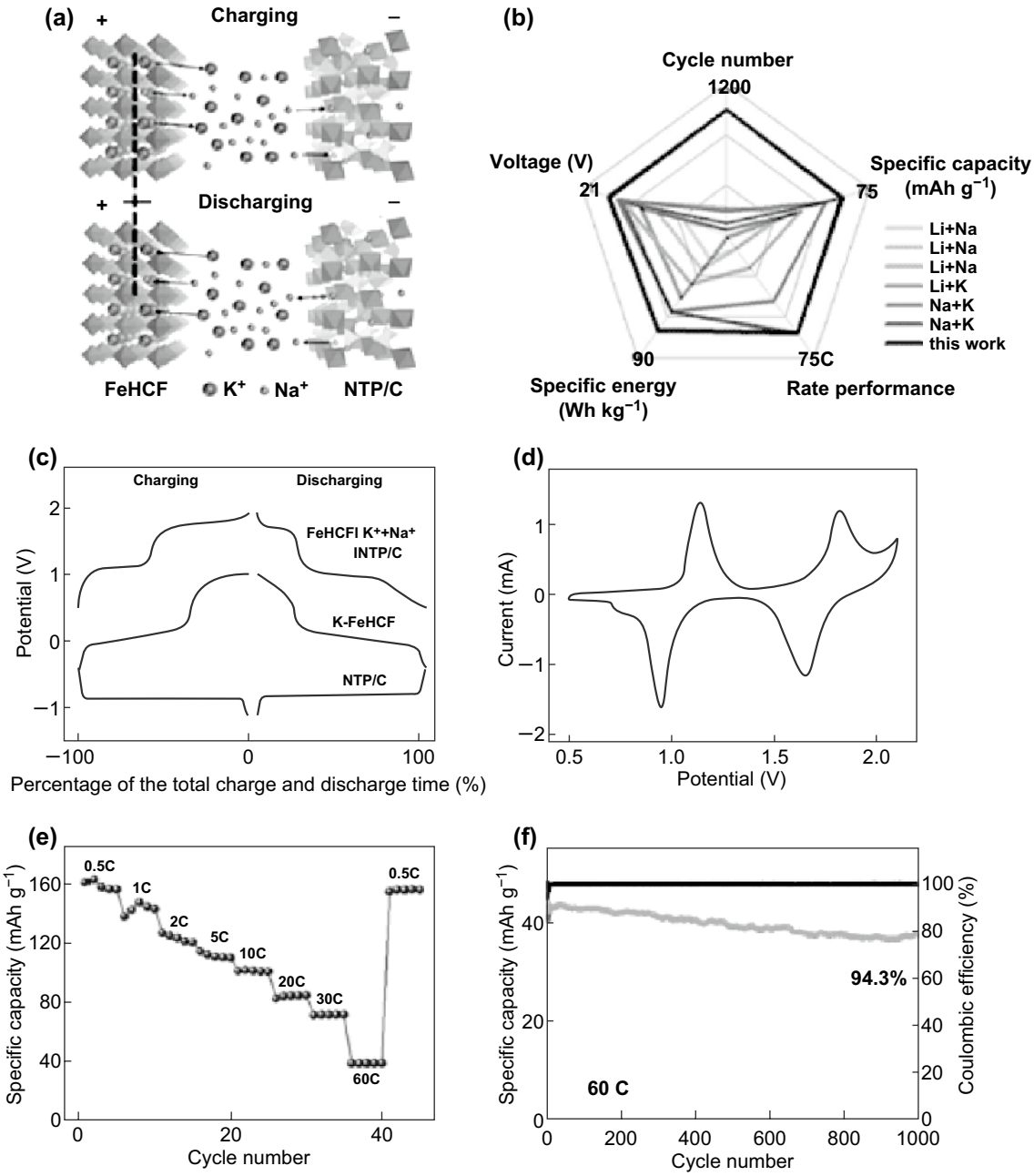

Fig. 11 **a** Schematic of the K–Na hybrid aqueous battery (HAB). **b** Performance comparison between the HAB designed in this work and other previously reported mixed-ion aqueous batteries. **c** Galvanostatic profiles of the HAB along with the voltage profiles of their individual anode and cathode electrodes versus SCE at the rate of 1 C. **d** CV curves of the HAB at the scan rate of 1 mVs^{-1}. **e** Rate performance of the HAB. **f** Long-term cycling stability of the HAB at the rate of 60 C [186]. Copyright 2018, Wiley-VCH Verlag

2.4 Aqueous Batteries with Desalination

New desalination technologies with high ion removal capacity and low energy consumption are urgently needed to solve the worldwide water scarcity problem, and capacitive deionization (CDI) is now regarded as a competitive electrochemical means of saving energy and delivering clean water, i.e., water desalination using energy storage electrode materials with the benefit of energy recovery [193–198]. Faradaic cation insertion electrodes (e.g., NTP, NMO) have

https://doi.org/10.1007/s40820-019-0273-1

been widely used in electrochemical energy storage and more recently have been explored for selective electrochemical deionization applications due to the higher inherent ion selectivity and lower energy/material intensity arising from their specific crystalline structures and well-defined redox potentials [21, 193, 199–204]. Depending on the consistency with the lattice vacancy in the host's crystal lattice, only smaller monovalent Li^+ and Na^+ ions may insert into the host compound's crystal lattice, while the larger monovalent ions (e.g., K^+) or divalent ions (e.g., Ca^{2+}) are left behind in the solution, and the removal capacities could be 5–10 time higher than carbon materials with high preference to specific inserting ions (Fig. 12a, b) [195, 198, 199]. Taking the NTP/rGO composite as an example, in the novel hybrid electrochemical deionization (EDI) system, Na^+ ions in the saline water will be intercalated into the NTP/rGO electrode via a chemical reaction, while Cl^- ions are physically adsorbed on the other AC electrode. The EDI system showed an ultrahigh desalination performance with an initial salt removal capacity of 140 mg g^{-1} at a current density of 100 mA g^{-1}, and retaining 120 mg g^{-1} over 100 cycles. A particularly rapid desalination rate of 0.45 mg g^{-1} s^{-1} can be achieved at 1000 mA g^{-1} with a removal capacity of 27 mg g^{-1} [22]. Through further replacement of the AC electrode with an Ag nanoparticles/rGO composite electrode, a lower-energy-consumption dual-ion electrochemical deionization system was designed, where NTP/rGO served as a Na^+ ion Faradaic electrode and Ag-NPs/rGO as a Cl^- ion Faradaic electrode. The estimated energy consumption can be as low as 0.254 Wh L^{-1} for the desalination of brackish water (2500 ppm) to drinkable water (500 ppm). However, because currently few materials can be chosen as an efficient anion Faradaic electrode, the development of cost-efficient battery materials will also accelerate desalination technology [204–207].

Further study showed that the ion transport from the bulk electrolyte to the electrode surface limited the rate of ion removal and the round-trip CE, and the presence of non-inserting ions in water would reduce the ionic flux and ion removal

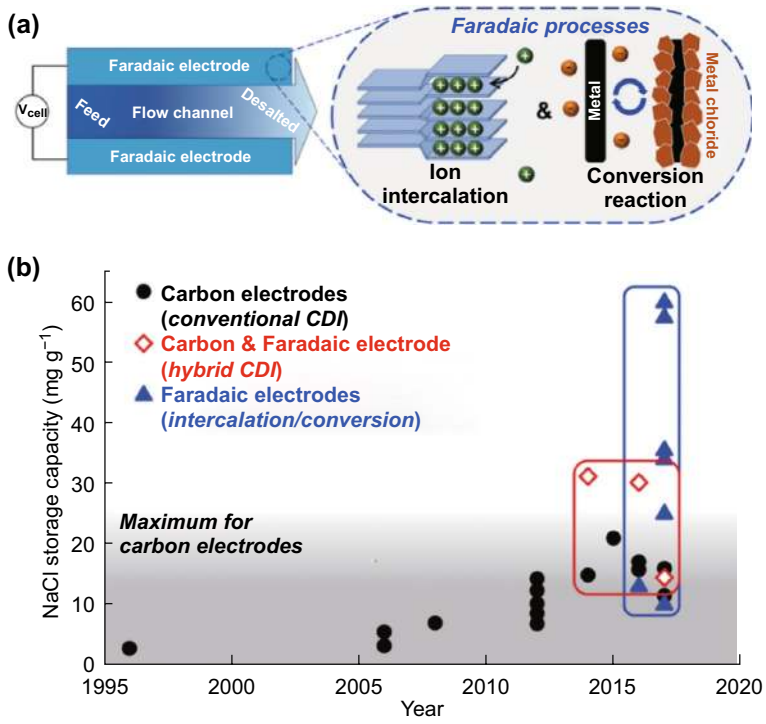

Fig. 12 Concept and performance values of capacitive deionization (CDI) cells with capacitive and Faradaic electrodes. Historical evolution of the salt storage capacity of desalination cells achieved with either nanoporous carbon electrodes (black circles), Faradaic electrodes (blue triangles), or hybrid cells with one nanoporous carbon electrode and one Faradaic electrode (red diamonds), with all values reported per mass of both electrodes. Despite their recent introduction, cells with Faradaic electrodes have achieved significantly higher gravimetric salt storage capacities compared with cells with nanoporous carbon electrodes. Schematics contrast the salt storage mechanism of CDI cells leveraging nanoporous carbon (capacitive) electrodes and cells with Faradaic electrodes, such as layered intercalation electrodes or conversion electrodes [195]. Copyright 2017, Elsevier Inc. (Color figure online)

capacity due to the containment of interfacial transport following the accumulation effect [199]. Generally, optimizing the operating current density and cutoff voltage window (to reduce the parasitic water splitting reaction) as well as advective ion transport to the electrode surface will improve the ion removal performance in dilute aqueous systems [199]. The excellent performance of the EDI system based on NTP composites has made it a promising desalination technology and provides significant potential for direct seawater desalination in the future. By combining commercial photovoltaics, the goal of "renewables to usable electric energy and desalted water" can be achieved [208].

Apart from the above-discussed SIBs, some other new types of energy storage systems such as Mg–Na hybrid ion batteries based on the NTP-based electrode have also been reported [185, 209, 210]. Mai's group first reported the novel NTP nanowire clusters as a hybrid magnesium–sodium-ion battery's cathode with the combined advantages of a fast alkali metal ions intercalation cathode and a dendrite-free Mg anode and exhibited good electrochemical performance with a high reversible capacity of 124 mAh g^{-1} at 1 C, considerable rate capability, and good cycling stability (Fig. 13c–e) [211]. As shown in Fig. 13a, b, this innovative device consists of an anode of Mg metal, a cathode of NTP nanowire clusters, and a dual salt electrolyte consisting of the common MIB electrolyte with a suitable Na salt added to it. Because of the open structure of the self-assembled NTP nanoarchitecture and the suitable potential of 1.7 V (vs. Mg/Mg^{2+}) of NTP, NTP nanowire clusters can be potentially used as the cathode for magnesium–sodium hybrid ion batteries.

3 Hybrid Capacitors

In the past few years, many articles on NHCs or hybrid sodium-ion capacitors (NICs, or SICs) have been published [37, 212–215]. Apart from the high-electrical-conductivity carbon-based materials and high-power-performance metal oxides such as TiO_2, Nb_2O_5 and so on, $NaTi_2(PO_4)_3$ with a NASICON structure features high ionic conductivity and structural stability with the excellent kinetics of sodium, and therefore will be a suitable material for sodium-ion hybrid capacitor applications [32, 212, 216, 217]. However, it has poor electron conductivity, and therefore many methods such as reducing the particle size, coating conductive materials, adopting suitable counter electrode materials, etc., have been used to rationally design NTP materials to solve these problems [218, 219].

Zhang and his coworkers first reported that a $NaTi_2(PO_4)_3$/C composite synthesized by the ball milling method used as the anode of an aqueous sodium-ion hybrid supercapacitor with AC as the cathode could deliver a high energy density of 31.6 Wh kg^{-1}. When tested at a current density of 200 mA g^{-1}, the cell delivered an excellent cycle performance of less than 11.7% capacitance loss after 2000 cycles. This electrochemical performance is derived from the unique structure of the as-synthesized $NaTi_2(PO_4)_3$/C composite. First, the NASICON structure of $NaTi_2(PO_4)_3$ could promote rapid and easy migration of Na^+ ions in the 3D open framework structure. On the other hand, the intimate mixing of acetylene black and sucrose with the precursor material through ball milling results in the formation of a uniform amorphous carbon layer of approximately 7 nm on the surface of the NTP particles so that the electron conductivity of the $NaTi_2(PO_4)_3$/C composite could be significantly improved [218]. However, the as-synthesized $NaTi_2(PO_4)_3$/C composite is in the range of 0.5–2 mm, which might be detrimental to the diffusion of ions and electrons in the electrode material. Roh et al. reported a $NaTi_2(PO_4)_3$/rGO microsphere composite synthesized by a facile spray-drying method used as a high-rate insertion anode for sodium-ion capacitors. The spray-drying method produced a structure of NTP nanoparticles with sizes < 80 nm, which considerably reduced the diffusion length of the Na^+ ion inside the material. Moreover, during the synthesis process, components of titanium were ionic species, which caused the chemical bonding of high-conductivity reduced graphene oxide (rGO) with NTP and finally significantly improved the electrical conductivity of the composite. When fabricated with an AC counter electrode to construct an NHC, a maximum energy density of 53 Wh kg^{-1} at a power density of 334 W kg^{-1} with good cycling stability was obtained [220].

Similar work has also been reported by Lee and his coworkers. They synthesized NTP nanoparticles grown on graphene nanosheets as an anode with the graphene nanosheets as a cathode in an organic electrolyte NHC. This new system features a high specific surface area and a high-conductivity nanosheet-like graphene cathode. Unlike the activated carbon electrode, which is porous with pores that are not conducive to electron transport, the surface of the 2D nanosheet

 https://doi.org/10.1007/s40820-019-0273-1

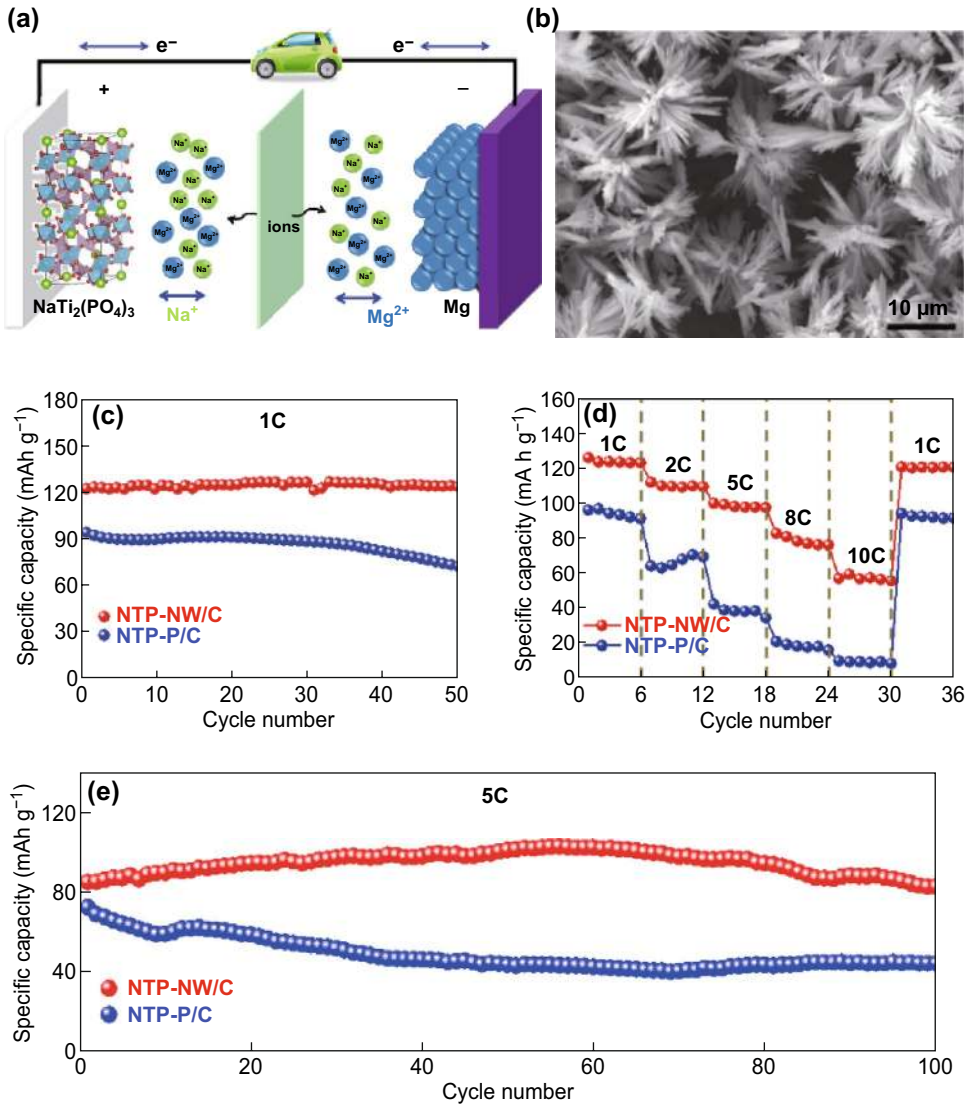

Fig. 13 **a** Schematic illustration of the Mg–Na hybrid battery in this work. **b** FESEM image of NTP-NW/C. **c** Cycling performances of NTP-NW/C and NTP-P/C at 1 C. **d** Rate performances of NTP-NW/C and NTP-P/C. **e** Cycling performances of NTP-NW/C and NTP-P/C at 5 C [211]. Copyright 2018, Elsevier Ltd

can be easily contacted by ions in the electrolyte, thereby reducing the ion transport distance. This new system delivers a high energy density of ≈ 80 Wh kg^{-1} and a high specific power of 8 kW kg^{-1}. An ultralow performance fading of ≈ 0.13% per 1000 cycle (90%–75,000 cycles) outperforms previously reported sodium-ion capacitors [32].

Electrospinning is a classic method of preparing a 3D network carbon nanofiber with uniform morphology and good electrical conductivity. Recently, Wei et al. reported that porous NTP/C nanofibers (NTP/CNFs) obtained via an electrospinning method's anode of NHCs could deliver a maximum specific energy density of 56 Wh kg^{-1} at a specific power density of 174 W kg^{-1}. At a current density of 1 A g^{-1}, the specific capacitance remained at 91.4% after 500 cycles with nearly 100% CE. The electrospinning method uniformly dispersed the NTP nanoparticles with an average crystal size of ~ 15 nm in the carbon matrix. Characterizations suggested that NTP/CNFs have a typical porous structure with a high specific surface area that will facilitate electrolyte infiltration and finally produce high electrochemical performance [75].

Recently, Wei et al. reported mesoporous NTP nanocages with iso-oriented tiny nanocrystals (Fig. 14a, b) synthesized by the solvothermal method used as the anode for an NHC. The full cell (with AC as the positive electrode, NTP nanocages as the anode, and 1 M $NaClO_4$ in PC as the electrolyte) combines the advantages of the batteries and supercapacitors, i.e., relative high capacitance, outstanding rate performance, and long cycling stability (with obvious humps between 0.9–1.6 V in CV curves due to the rapid insertion/extraction of Na^+ with the NTP electrode accompanied by the adsorption/desorption of $NaClO_4^-$ with the AC electrode, corresponding to the well-matched stable charge–discharge profiles) (Fig. 14c–f). It could deliver an energy density of 56 Wh kg^{-1} at a power density of 39 W kg^{-1} and excellent cycle performance without obvious capacity degradation after 20,000 cycles even at a high current rate of 5 A g^{-1}. SEM and TEM images show that the products display a hollow structure with cube-like morphologies in the range 20–50 nm. The N_2 sorption isotherm confirmed the porous nanostructures with a specific surface area of

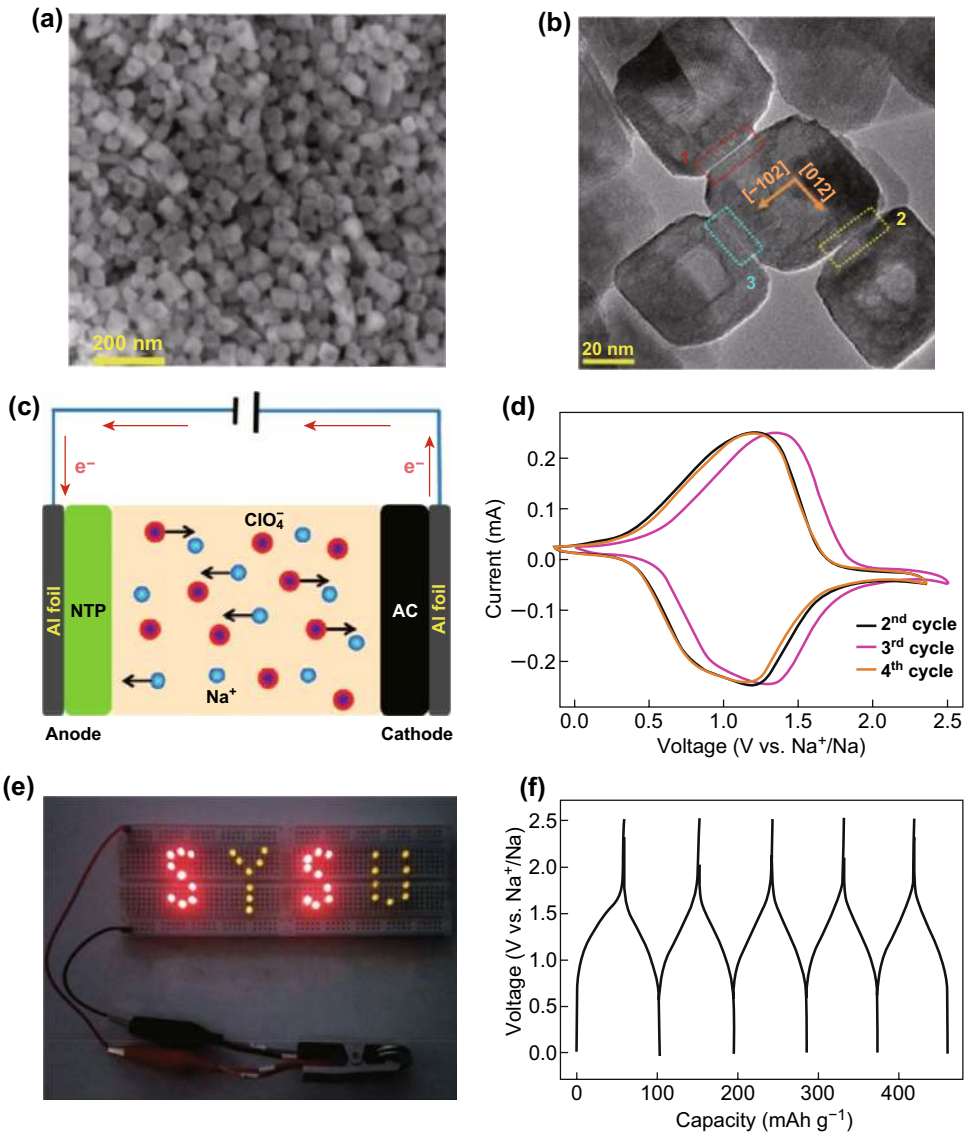

Fig. 14 **a** SEM and **b** TEM images of the obtained mesoporous NTP nanocages. **c** Schematic illustration of the operating mechanism of an NHC. **d** Photograph of a logo consisting of 35 LEDs powered by two NHCs in series. **e**, **f** CV curves and charge–discharge profiles of the sodium-ion capacitor [221]. Copyright 2017, American Chemical Society

https://doi.org/10.1007/s40820-019-0273-1

67.4 m^2 g^{-1}; such a unique porous nanostructure results in more active sites, shorter ion transport routes, and finally promotes sodium-ion transport dynamics [221]. With the merits of impressive energy and power densities as well as cycling performance, the hybrid capacitor could be a promising device for high-efficiency energy storage systems.

After this work, Yang and his coworkers synthesized a porous single-crystal NTP by liquid transformation of ultrathin TiO_2 nanosheets, followed by mixing with phenolic resin and calcining in an inert atmosphere to coat the conductive carbon sheath (denoted by PSC-NTP@C) (Fig. 15a, b). By comparing with partially crystallographic solid spheres that were NTP-fabricated via liquid transformation before annealing, the mesopores were determined to be derived from shrinking of amorphous nanodomains. The high crystallinity results in a more robust structure that enabled NTP to store sodium ions without causing large lattice stresses, finally helping improve cycle performance; at the same time, the thin amorphous carbon layer confirmed by TEM images could improve the efficiency of ion transfer in the electrode, resulting in excellent high rate performance, outstanding safety, and excellent flexibility [38]. When coupled with ZIF-8 derived N-doped porous carbon (NC) as the cathode material to assemble an aqueous Na-ion

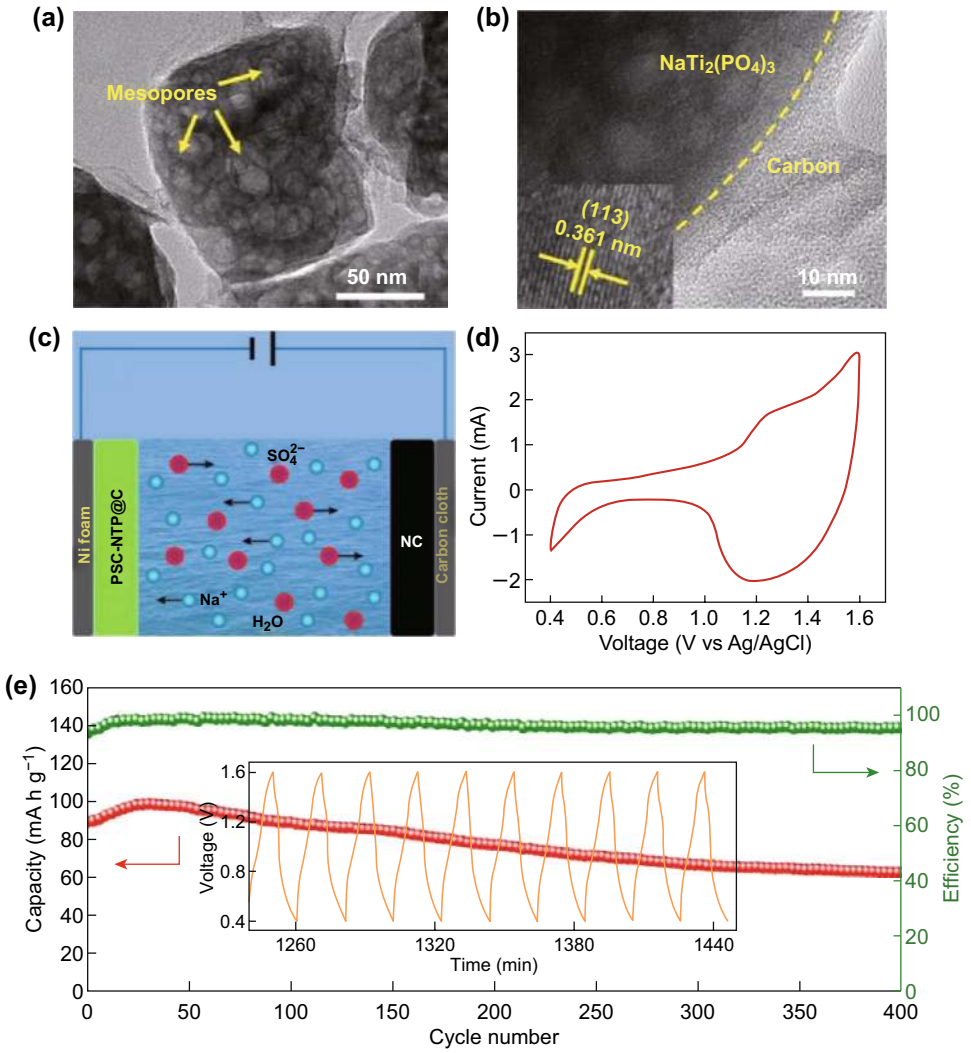

Fig. 15 **a** TEM image reveals the porous nanostructure of single-crystal $NaTi_2(PO_4)_3$ coated with amorphous carbon layer (PSC-NTP@C); **b** HRTEM image at the interface between an NTP and the carbon layer. **c** Schematic illustration of the PSC-NTP@C//NC Na-ion capacitor in liquid aqueous electrolyte; **d** CV curve of this Na-ion capacitor recorded at 3 mV s^{-1} within a cutoff voltage window of 0.4–1.6 V. **e** Cycle performance of the PSC-NTP@C//NC system at 0.5 A g^{-1} (the inset shows the voltage–time profile) [38]. Copyright 2018, Elsevier Ltd

capacitor, the majority of the capacitance existed in the range 1.0–1.6 V for the PSC-NTP@C//NC capacitor, which showed a high initial discharge capacity of ~ 90 mAh g^{-1}, good cycle stability, and high reversibility (Fig. 15c–e). It could further be fabricated to a flexible quasi-solid-state Na-ion capacitor with a sandwich structure, showing superior bendability for aqueous energy storage systems.

4 Conclusion and Perspectives

In summary, the NASICON-type NTP-based electrode materials with exceptionally high ion conductivity and pronounced structural stability overcome the multiple kinetic problems of Na-ion systems, facilitating low-cost large-scale electrochemical energy storage with inhibited capacity decay, higher rate capacities, and CEs. When paired with existing competent cathodes, the class of NTP anode materials for SIBs shows advantages comparable with or superior to commercial high-power LIBs. Furthermore, among the many cutting-edge anode materials identified to deliver promising results, with some outperforming their lithium equivalents, NTP demonstrates a zero-strain insertion feature as well as a high ICE and a relatively high Na insertion/deinsertion, avoiding the formation of SEI and ensuring the safety of large-scale and high-power batteries [58]. The full volume change of the NTP anode with other paired cathodes is almost zero because they share approximately the same but inverse volume change during charging and discharging, which facilitates the realization of safe, long-term cyclability and flexible structure design for large-capacity batteries. On the basis of the above encouraging results, it is concluded that SIBs (including aqueous and non-aqueous), as well as NHCs, have shown significant potential for commercialization in the near future while there is plenty of room for the development of energy storage devices with higher energy densities and long-term lifespan. These areas should be the focus for future relevant research as follows:

1. Despite the fact that NTP has considerable potential for the development of high-performance SIBs, due to its relatively high voltage plateau as anodes, when used for a full cell, it will require cathodes with a high discharge potential to match and realize high power output. Thus, a higher technological requirement for the cathode materials should be proposed [45, 85, 107, 222]. From the viewpoint of practical battery applications, a high tap density is desirable for higher energy density in addition to high-power performance. In addition, the self-discharge rate has not been systematically evaluated, compared to the typical commercial LIBs with a value of 2% per month; the NTP-based SIBs and NHCs should be further investigated for practical application.
2. Although the ASIBs are more cost-effective and safer for large-scale energy storage, they often have a lower capacity and cycling life compared to that of organic SIBs. Because capacity fade in aqueous electrolytes remains poorly understood, further studies are needed, including a possible multi-step mechanism followed by a local pH change and alkaline oxidation of the carbon conductive additives [148].
3. The decay mechanism and stability of electrode materials in an aqueous electrolyte should be further studied and improved, although some efforts have shown promise by tailoring the electrolytes (including adjusting the pH values, locally generated destructive OH^- ions), nanocoating the electrode materials, or eliminating oxygen in the electrolytes to suppress capacity fading upon cycling. An appropriate potential window (cutoff voltage) and corresponding anode and cathode materials (with adjusted mass ratio) should be selected to avoid or suppress the highly irreversible capacity loss due to H_2 and/or O_2 evolution in the aqueous electrolytes.
4. For alternative electrolytes, the intrinsically safe organic phosphates for all-phosphate SIBs efficiently avoid firing as usually encountered in the carbonate electrolytes and severe side reactions such as hydrogen and oxygen evolution in aqueous electrolytes. The all-solid-state SIBs with safety, long-term operation capacity, and high-temperature performance advantages show considerable commercial potential. However, more related research on the interface contact is necessary, and the cycling performance of these batteries needs to be further improved for wide practical application.
5. The realization of full cell SIBs or hybrid Na-ion capacitors with high energy and long cycle life remains challenging. The controlled formation of an SEI on both anodes (especially for the hard-carbon-incorporated composites) and cathodes will be an effective way to achieve long-term stability for full cells. Pre-cycling (or pre-sodiation) of anodes and cathodes will lead to pre-formation of SEI, and hence mitigate the additional consumption of Na ions in full cells for higher ICE as well. With the improvement in aqueous electrolytes, including highly concentrated and even superconcentrated WiSEs or hybrid aqueous/non-aqueous electrolytes, the prospects are promising for large-scale and high-energy-density electrochemical energy storage with the advantages of low cost, eco-friendliness, and long lifespan.

https://doi.org/10.1007/s40820-019-0273-1

6. Compared to conventional SIBs relayed on Cu/Al current collectors to support active materials and to serve as conductive pathways, free-standing or flexible electrodes (including graphene papers, graphene foams, and electrospun CNFs) without these metallic current collectors significantly reduce the weight and cost of batteries and have been an emerging demand for today's battery development. However, more efforts are needed to develop better-performing free-standing electrode materials with a facile preparation route, low cost, and robust mechanical advantages for next-generation batteries.
7. Compared with traditional static capacitive deionization (CDI) using carbon electrodes, Faradaic capacitive (intercalation) electrodes including NTP can remove ion species with high efficiency (typically, an ultrahigh salt removal capacity of more than 100 mg g^{-1}). These electrodes are promising for not only being a commercially viable alternative for treating water but also for saving energy. However, the stability of these electrodes (particularly associated with electrochemical leakage of metal ions) may be currently a major concern. Furthermore, it is necessary to develop robust and cost-effective intercalation cathodes and anodes to meet the critical requirement of capturing multiple cations and anions from real saline water or seawater.

Acknowledgements This work was supported by the National Natural Science Foundation of China (No. 51302079), the Natural Science Foundation of Hunan Province (No. 2017JJ1008), and theKey Research and Development Program of Hunan Province of China under Grant 2018GK2031.

Electronic supplementary material The online version of this article (https://doi.org/10.1007/s40820-019-0273-1) contains supplementary material, which is available to authorized users.

References

1. S. Chu, A. Majumdar, Opportunities and challenges for a sustainable energy future. Nature **488**(7411), 294–303 (2012). https://doi.org/10.1038/nature11475
2. S. Chu, Y. Cui, N. Liu, The path towards sustainable energy. Nat. Mater. **16**, 16–22 (2016). https://doi.org/10.1038/nmat4834
3. X. Zhang, X. Cheng, Q. Zhang, Nanostructured energy materials for electrochemical energy conversion and storage: a review. J. Energy Chem. **25**(6), 967–984 (2016). https://doi.org/10.1016/j.jechem.2016.11.003
4. S. Qi, D. Wu, Y. Dong, J. Liao, C.W. Foster, C. O'Dwyer, Y. Feng, C. Liu, J. Ma, Cobalt-based electrode materials for sodium-ion batteries. Chem. Eng. J. **370**, 185–207 (2019). https://doi.org/10.1016/j.cej.2019.03.166
5. F. Li, Z. Wei, Y. Feng, J. Ma, L. Mai, Sodium-based batteries: from critical materials to battery systems. J. Mater. Chem. A **7**, 9406–9943 (2019). https://doi.org/10.1039/c8ta11999f
6. L. Wang, Y. Wang, M. Wu, Z. Wei, C. Cui et al., Nitrogen, fluorine, and boron ternary doped carbon fibers as cathode electrocatalysts for zinc–air batteries. Small **14**(20), 1800737 (2018). https://doi.org/10.1002/smll.201800737
7. S. Qi, L. Mi, K. Song, K. Yang, J. Ma, X. Feng, J. Zhang, W. Chen, Understanding shuttling effect in sodium ion batteries for the solution of capacity fading: FeS_2 as an example. J. Phys. Chem. C **123**(5), 2775–2782 (2019). https://doi.org/10.1021/acs.jpcc.8b11069
8. J. Liu, J. Liang, C. Wang, J. Ma, Electrospun CoSe@ N-doped carbon nanofibers with highly capacitive Li storage. J. Energy Chem. **33**, 160–166 (2019). https://doi.org/10.1016/j.jechem.2018.09.006
9. J. Liao, R. Tan, Z. Kuang, C. Cui, Z. Wei et al., Controlling the morphology, size and phase of Nb_2O_5 crystals for high electrochemical performance. Chin. Chem. Lett. **29**(12), 1785–1790 (2018). https://doi.org/10.1016/j.cclet.2018.11.018
10. W. Zhang, W.K. Pang, V. Sencadas, Z. Guo, Understanding high-energy-density Sn_4P_3 anodes for potassium-ion batteries. Joule **2**(8), 1534–1547 (2018). https://doi.org/10.1016/j.joule.2018.04.022
11. R. Schmuch, R. Wagner, G. Hörpel, T. Placke, M. Winter, Performance and cost of materials for lithium-based rechargeable automotive batteries. Nat. Energy **3**(4), 267–278 (2018). https://doi.org/10.1038/s41560-018-0107-2
12. B. Dunn, H. Kamath, J.M. Tarascon, Electrical energy storage for the grid: a battery of choices. Science **334**(6058), 928–935 (2011). https://doi.org/10.1126/science.1212741
13. L. Yu, L.P. Wang, H. Liao, J. Wang, Z. Feng et al., Understanding fundamentals and reaction mechanisms of electrode materials for Na-ion batteries. Small **14**(16), 1703338 (2018). https://doi.org/10.1002/smll.201703338
14. J.-Y. Hwang, S.-T. Myung, Y.-K. Sun, Sodium-ion batteries: present and future. Chem. Soc. Rev. **46**(12), 3529–3614 (2017). https://doi.org/10.1039/c6cs00776g
15. J. Cui, S. Yao, J.-K. Kim, Recent progress in rational design of anode materials for high-performance Na-ion batteries. Energy Storage Mater. **7**, 64–114 (2017). https://doi.org/10.1016/j.ensm.2016.12.005

16. A. Bauer, J. Song, S. Vail, W. Pan, J. Barker, Y. Lu, The scale-up and commercialization of nonaqueous Na-ion battery technologies. Adv. Energy Mater. **8**(17), 1702869 (2018). https://doi.org/10.1002/aenm.201702869
17. J. Deng, W.B. Luo, S.L. Chou, H.K. Liu, S.X. Dou, Sodium-ion batteries: from academic research to practical commercialization. Adv. Energy Mater. **8**(4), 1701428 (2018). https://doi.org/10.1002/aenm.201701428
18. Y. Huang, Y. Zheng, X. Li, F. Adams, W. Luo, Y. Huang, L. Hu, Electrode materials of sodium-ion batteries toward practical application. ACS Energy Lett. **3**(7), 1604–1612 (2018). https://doi.org/10.1021/acsenergylett.8b00609
19. Y. Li, Y. Lu, C. Zhao, Y.-S. Hu, M.-M. Titirici, H. Li, X. Huang, L. Chen, Recent advances of electrode materials for low-cost sodium-ion batteries towards practical application for grid energy storage. Energy Storage Mater. **7**, 130–151 (2017). https://doi.org/10.1016/j.ensm.2017.01.002
20. N. Wang, C. Chu, X. Xu, Y. Du, J. Yang, Z. Bai, S. Dou, Comprehensive new insights and perspectives into Ti-based anodes for next-generation alkaline metal (Na+ , K+) ion batteries. Adv. Energy Mater. **8**(27), 1801888 (2018). https://doi.org/10.1002/aenm.201801888
21. J. Lee, S. Kim, C. Kim, J. Yoon, Hybrid capacitive deionization to enhance the desalination performance of capacitive techniques. Energy Environ. Sci. **7**(11), 3683–3689 (2014). https://doi.org/10.1039/c4ee02378a
22. Y. Huang, F. Chen, L. Guo, H.Y. Yang, Ultrahigh performance of a novel electrochemical deionization system based on a $NaTi_2(PO_4)_3$/rGO nanocomposite. J. Mater. Chem. A **5**(34), 18157–18165 (2017). https://doi.org/10.1039/c7ta03725b
23. M.Á. Muñoz-Márquez, D. Saurel, J.L. Gómez-Cámer, M. Casas-Cabanas, E. Castillo-Martínez, T. Rojo, Na-ion batteries for large scale applications: a review on anode materials and solid electrolyte interphase formation. Adv. Energy Mater. **7**(20), 1700463 (2017). https://doi.org/10.1002/aenm.201700463
24. Y.Q. Luo, Y.J. Tang, S.S. Zheng, Y. Yan, H.Q. Xue, H. Pang, Dual anode materials for lithium- and sodium-ion batteries. J. Mater. Chem. A **6**(10), 4236–4259 (2018). https://doi.org/10.1039/c8ta00107c
25. S. Chen, C. Wu, L. Shen, C. Zhu, Y. Huang, K. Xi, J. Maier, Y. Yu, Challenges and perspectives for NASICON-type electrode materials for advanced sodium-ion batteries. Adv. Mater. **29**(48), 1700431 (2017). https://doi.org/10.1002/adma.201700431
26. J. Mao, T. Zhou, Y. Zheng, H. Gao, H.K. Liu, Z. Guo, Two-dimensional nanostructures for sodium-ion battery anodes. J. Mater. Chem. A **6**(8), 3284–3303 (2018). https://doi.org/10.1039/C7TA10500B
27. Z. Wei, L. Wang, M. Zhuo, W. Ni, H. Wang, J. Ma, Layered tin sulfide and selenide anode materials for Li- and Na-ion batteries. J. Mater. Chem. A **6**(26), 12185–12214 (2018). https://doi.org/10.1039/C8TA02695E
28. L. Yu, H. Hu, H.B. Wu, X.W. Lou, Complex hollow nanostructures: synthesis and energy-related applications. Adv. Mater. **29**(15), 1604563 (2017). https://doi.org/10.1002/adma.201604563
29. S.Y. Hong, Y. Kim, Y. Park, A. Choi, N.-S. Choi, K.T. Lee, Charge carriers in rechargeable batteries: Na ions vs. Li ions. Energy Environ. Sci. **6**(7), 2067–2081 (2013). https://doi.org/10.1039/c3ee40811f
30. Y. Jiao, J. Pei, D. Chen, C. Yan, Y. Hu, Q. Zhang, G. Chen, Mixed-metallic MOF based electrode materials for high performance hybrid supercapacitors. J. Mater. Chem. A **5**(3), 1094–1102 (2017). https://doi.org/10.1039/c6ta09805c
31. P. Simon, Y. Gogotsi, Capacitive energy storage in nanostructured carbon-electrolyte systems. Acc. Chem. Res. **46**(5), 1094–1103 (2013). https://doi.org/10.1021/ar200306b
32. R. Thangavel, B. Moorthy, D.K. Kim, Y.S. Lee, Pushing the energy output and cyclability of sodium hybrid capacitors at high power to new limits. Adv. Energy Mater. **7**(14), 1602654 (2017). https://doi.org/10.1016/j.jechem.2016.11.003
33. Z. Lin, E. Goikolea, A. Balducci, K. Naoi, P. Taberna, M. Salanne, G. Yushin, P. Simon, Materials for supercapacitors: when Li-ion battery power is not enough. Mater. Today **21**(4), 419–436 (2018). https://doi.org/10.1016/j.mattod.2018.01.035
34. F. Wang, X. Wu, X. Yuan, Z. Liu, Y. Zhang et al., Latest advances in supercapacitors: from new electrode materials to novel device designs. Chem. Soc. Rev. **46**(22), 6816–6854 (2017). https://doi.org/10.1039/c8ta02416b
35. J. Liu, J. Wang, C. Xu, H. Jiang, C. Li, L. Zhang, J. Lin, Z.X. Shen, Advanced energy storage devices: basic principles, analytical methods, and rational materials design. Adv. Sci. **5**(1), 1700322 (2018). https://doi.org/10.1002/advs.201700322
36. Y. Shao, M.F. El-Kady, J. Sun, Y. Li, Q. Zhang, M. Zhu, H. Wang, B. Dunn, R.B. Kaner, Design and mechanisms of asymmetric supercapacitors. Chem. Rev. **118**(18), 9233–9280 (2018). https://doi.org/10.1021/acs.chemrev.8b00252
37. H. Wang, C. Zhu, D. Chao, Q. Yan, H.J. Fan, Nonaqueous hybrid lithium-ion and sodium-ion capacitors. Adv. Mater. **29**(46), 1702093 (2017). https://doi.org/10.1002/adma.201702093
38. Q. Yang, S. Cui, Y. Ge, Z. Tang, Z. Liu et al., Porous single-crystal $NaTi_2(PO_4)_3$ via liquid transformation of TiO_2 nanosheets for flexible aqueous Na-ion capacitor. Nano Energy **50**, 623–631 (2018). https://doi.org/10.1016/j.nanoen.2018.06.017
39. Z. Jian, Y.S. Hu, X. Ji, W. Chen, Nasicon-structured materials for energy storage. Adv. Mater. **29**(20), 1601925 (2017). https://doi.org/10.1002/adma.201601925
40. Y. Xu, Q. Wei, C. Xu, Q. Li, Q. An, P. Zhang, J. Sheng, L. Zhou, L. Mai, Layer-by-layer $Na_3V_2(PO_4)_3$ embedded in reduced graphene oxide as superior rate and ultralong-life sodium-ion battery cathode. Adv. Energy Mater. **6**(14), 1600389 (2016). https://doi.org/10.1002/aenm.201600389
41. C. Xu, Y. Xu, C. Tang, Q. Wei, J. Meng, L. Huang, L. Zhou, G. Zhang, L. He, L. Mai, Carbon-coated hierarchical $NaTi_2(PO_4)_3$ mesoporous microflowers with superior sodium

 https://doi.org/10.1007/s40820-019-0273-1

storage performance. Nano Energy **28**, 224–231 (2016). https://doi.org/10.1016/j.nanoen.2016.08.026

42. Q. Ni, Y. Bai, F. Wu, C. Wu, Polyanion-type electrode materials for sodium-ion batteries. Adv. Sci. **4**(3), 1600275 (2017). https://doi.org/10.1002/advs.201600275
43. Z. Li, D. Young, K. Xiang, W.C. Carter, Y.M. Chiang, Towards high power high energy aqueous sodium-ion batteries: the $NaTi_2(PO_4)_3/Na_{0.44}MnO_2$ system. Adv. Energy Mater. **3**(3), 290–294 (2013). https://doi.org/10.1002/aenm.201200598
44. Y. Fang, L. Xiao, J. Qian, Y. Cao, X. Ai, Y. Huang, H. Yang, 3D graphene decorated $NaTi_2(PO_4)_3$ microspheres as a superior high-rate and ultracycle-stable anode material for sodium ion batteries. Adv. Energy Mater. **6**(19), 1502197 (2016). https://doi.org/10.1002/aenm.201502197
45. C. Wu, P. Kopold, Y.-L. Ding, P.A. van Aken, J. Maier, Y. Yu, Synthesizing porous $NaTi_2(PO_4)_3$ nanoparticles embedded in 3D graphene networks for high-rate and long cycle-life sodium electrodes. ACS Nano **9**(6), 6610–6618 (2015). https://doi.org/10.1021/acsnano.5b02787
46. X. Wu, Y. Cao, X. Ai, J. Qian, H. Yang, A low-cost and environmentally benign aqueous rechargeable sodium-ion battery based on $NaTi_2(PO_4)_3$–$Na_2NiFe(CN)_6$ intercalation chemistry. Electrochem. Commun. **31**, 145–148 (2013). https://doi.org/10.1016/j.elecom.2013.03.013
47. S.I. Park, I. Gocheva, S. Okada, J.-I. Yamaki, Electrochemical properties of $NaTi_2(PO_4)_3$ anode for rechargeable aqueous sodium-ion batteries. J. Electrochem. Soc. **158**(10), A1067–A1070 (2011). https://doi.org/10.1149/1.3611434
48. G. Yang, H. Song, M. Wu, C. Wang, Porous $NaTi_2(PO_4)_3$ nanocubes: a high-rate nonaqueous sodium anode material with more than 10000 cycle life. J. Mater. Chem. A **3**(36), 18718–18726 (2015). https://doi.org/10.1039/c5ta04491j
49. L. Zhang, X. Wang, W. Deng, X. Zang, C. Liu et al., An open holey structure enhanced rate capability in a $NaTi_2(PO_4)_3$/C nanocomposite and provided ultralong-life sodium-ion storage. Nanoscale **10**(3), 958–963 (2018). https://doi.org/10.1039/c7nr07000d
50. C. Delmas, F. Cherkaoui, A. Nadiri, P. Hagenmuller, A nasicon-type phase as intercalation electrode—$NaTi_2(PO_4)_3$. Mater. Res. Bull. **22**(5), 631–639 (1987). https://doi.org/10.1016/0025-5408(87)90112-7
51. P. Senguttuvan, G. Rousse, M. Arroyo, Y. De Dompablo, H. Vezin, J.-M. Tarascon, M. Palacín, Low-potential sodium insertion in a nasicon-type structure through the Ti (III)/Ti (II) redox couple. J. Am. Chem. Soc. **135**(10), 3897–3903 (2013). https://doi.org/10.1021/ja311044t
52. H. Kabbour, D. Coillot, M. Colmont, C. Masquelier, O. Mentré, α-Na_3M_2 $(PO_4)_3$ (M=Ti, Fe): absolute cationic ordering in NASICON-type phases. J. Am. Chem. Soc. **133**(31), 11900–11903 (2011). https://doi.org/10.1021/ja204321y
53. J. Liu, J. Zhang, S. Cheng, Z. Liu, B. Han, DNA-mediated synthesis of microporous single-crystal-like $NaTi_2(PO_4)_3$ nanospheres. Small **4**(11), 1976–1979 (2008). https://doi.org/10.1002/smll.200800284
54. H. Guler, F. Kurtulus, A rapid synthesis of sodium titanium phosphate, $NaTi_2(PO_4)_3$ by using microwave energy. Mater. Chem. Phys. **99**(2–3), 394–397 (2006). https://doi.org/10.1016/j.matchemphys.2005.11.011
55. R. Velchuri, B.V. Kumar, V.R. Devi, S.I. Seok, M. Vithal, Low temperature preparation of $NaTi_2(PO_4)_3$ by sol–gel method. Int. J. Nanotechnol. **7**(9–12), 1077–1086 (2010). https://doi.org/10.1504/ijnt.2010.034712
56. D. Ribero, K.C. Seymour, W.M. Kriven, Synthesis of $NaTi_2(PO_4)_3$ by the inorganic-organic steric entrapment method and its thermal expansion behavior. J. Am. Ceram. Soc. **99**(11), 3586–3593 (2016). https://doi.org/10.1111/jace.14420
57. M. Vujkovic, M. Mitric, S. Mentus, High-rate intercalation capability of $NaTi_2(PO_4)_3$/C composite in aqueous lithium and sodium nitrate solutions. J. Power Sources **288**, 176–186 (2015). https://doi.org/10.1016/j.jpowsour.2015.04.132
58. G. Pang, P. Nie, C. Yuan, L. Shen, X. Zhang, H. Li, C. Zhang, Mesoporous $NaTi_2(PO_4)_3$/CMK-3 nanohybrid as anode for long-life Na-ion batteries. J. Mater. Chem. A **2**(48), 20659–20666 (2014). https://doi.org/10.1039/c4ta04732j
59. G. Pang, C. Yuan, P. Nie, B. Ding, J. Zhu, X. Zhang, Synthesis of nasicon-type structured $NaTi_2(PO_4)_3$-graphene nanocomposite as an anode for aqueous rechargeable Na-ion batteries. Nanoscale **6**(12), 6328–6334 (2014). https://doi.org/10.1039/c3nr06730k
60. Y. Jiang, L. Zeng, J. Wang, W. Li, F. Pan, Y. Yu, A carbon coated nasicon structure material embedded in porous carbon enabling superior sodium storage performance: $NaTi_2(PO_4)_3$ as an example. Nanoscale **7**(35), 14723–14729 (2015). https://doi.org/10.1039/c5nr03978a
61. J. Song, S. Park, J. Gim, V. Mathew, S. Kim, J. Jo, S. Kim, J. Kim, High rate performance of a $NaTi_2(PO_4)_3$/rGO composite electrode via pyro synthesis for sodium ion batteries. J. Mater. Chem. A **4**(20), 7815–7822 (2016). https://doi.org/10.1039/c6ta02720b
62. L. Fu, X. Xue, Y. Tang, D. Sun, H. Xie, H. Wang, Size controlling and surface engineering enable $NaTi_2(PO_4)_3$/C outstanding sodium storage properties. Electrochim. Acta **289**, 21–28 (2018). https://doi.org/10.1016/j.electacta.2018.09.024
63. M. Sun, X. Han, S. Chen, $NaTi_2(PO_4)_3$@C nanoparticles embedded in 2D sulfur-doped graphene sheets as high-performance anode materials for sodium energy storage. Electrochim. Acta **289**, 131–138 (2018). https://doi.org/10.1016/j.electacta.2018.08.061
64. Y. Niu, M. Xu, Y. Zhang, J. Han, Y. Wang, C.M. Li, Detailed investigation of a $NaTi_2(PO_4)_3$ anode prepared by pyro-synthesis for Na-ion batteries. RSC Adv. **6**(51), 45605–45611 (2016). https://doi.org/10.1039/c6ra06533c
65. J.S. Ko, C.S. Choi, B. Dunn, J.W. Long, Electrochemical characterization of Na-ion charge-storage properties for nanostructured $NaTi_2(PO_4)_3$ as a function of crystalline order. J. Electrochem. Soc. **164**(9), A2124–A2130 (2017). https://doi.org/10.1149/2.1391709jes
66. X. Yang, K. Wang, X. Wang, G. Chang, S. Sun, Carbon-coated $NaTi_2(PO_4)_3$ composite: a promising anode material

for sodium-ion batteries with superior Na-storage performance. Solid State Ionics **314**, 61–65 (2018). https://doi.org/10.1016/j.ssi.2017.11.016

67. D. Cai, B. Qu, H. Zhan, Porous $NaTi_2(PO_4)_3$ nanoparticles coated with a thin carbon layer for sodium-ion batteries with enhanced rate and cycling performance. Mater. Lett. **218**, 14–17 (2018). https://doi.org/10.1016/j.matlet.2018.01.131
68. D. Xu, P. Wang, R. Yang, Nitrogen-doped carbon decorated $NaTi_2(PO_4)_3$ composite as an anode for sodium-ion batteries with outstanding electrochemical performance. Ceram. Int. **44**(6), 7159–7164 (2018). https://doi.org/10.1016/j.ceramint.2018.01.160
69. D. Wang, Q. Liu, C. Chen, M. Li, X. Meng et al., Nasicon-structured $NaTi_2(PO_4)_3$@C nanocomposite as the low operation-voltage anode material for high-performance sodium ion batteries. ACS Appl. Mater. Interfaces. **8**(3), 2238–2246 (2016). https://doi.org/10.1021/acsami.5b11003
70. L. Chen, J. Liu, Z. Guo, Y. Wang, C. Wang, Y. Xia, Electrochemical profile of $LiTi_2(PO_4)_3$ and $NaTi_2(PO_4)_3$ in lithium, sodium or mixed ion aqueous solutions. J. Electrochem. Soc. **163**(6), A904–A910 (2016). https://doi.org/10.1149/2.0531606jes
71. H. Liu, Y. Liu, 1d mesoporous $NaTi_2(PO_4)_3$/carbon nanofiber: the promising anode material for sodium-ion batteries. Ceram. Int. **44**(5), 5813–5816 (2018). https://doi.org/10.1016/j.ceramint.2017.12.147
72. M. Li, L. Liu, P. Wang, J. Li, Q. Leng, G. Cao, Highly reversible sodium-ion storage in $NaTi_2(PO_4)_3$/C composite nanofibers. Electrochim. Acta **252**, 523–531 (2017). https://doi.org/10.1016/j.electacta.2017.09.020
73. Q. Hu, M. Yu, J. Liao, Z. Wen, C. Chen, Porous carbon-coated $NaTi_2(PO_4)_3$ with superior rate and low-temperature properties. J. Mater. Chem. A **6**(5), 2365–2370 (2018). https://doi.org/10.1039/c7ta10207k
74. H. Liu, H. Zhang, C. Su, X. Li, Y. Guo, Three-dimensional $NaTi_2(PO_4)_3$@C microsphere as a high-performance anode material for advanced sodium-ion batteries. Solid State Ionics **322**, 79–84 (2018). https://doi.org/10.1016/j.ssi.2018.05.005
75. P. Wei, Y. Liu, Z. Wang, Y. Huang, Y. Jin et al., Porous $NaTi_2(PO_4)_3$/C hierarchical nanofibers for ultrafast electrochemical energy storage. ACS Appl. Mater. Interfaces. **10**(32), 27039–27046 (2018). https://doi.org/10.1021/acsami.8b08415
76. S. Yu, Y. Wan, C. Shang, Z. Wang, L. Zhou, J. Zou, H. Cheng, Z. Lu, Ultrafine $NaTi_2(PO_4)_3$ nanoparticles encapsulated in N-CNFs as ultra-stable electrode for sodium storage. Front. Chem. **6**, 270 (2018). https://doi.org/10.3389/fchem.2018.00270
77. Z. Huang, L. Liu, L. Yi, W. Xiao, M. Li et al., Facile solvothermal synthesis of $NaTi_2(PO_4)_3$/C porous plates as electrode materials for high-performance sodium ion batteries. J. Power Sources **325**, 474–481 (2016). https://doi.org/10.1016/j.jpowsour.2016.06.066
78. Y. Niu, M. Xu, C. Guo, C.M. Li, Pyro-synthesis of a nanostructured $NaTi_2(PO_4)_3$/C with a novel lower voltage plateau for rechargeable sodium-ion batteries. J. Colloid Interf. Sci. **474**, 88–92 (2016). https://doi.org/10.1016/j.jcis.2016.04.021
79. G.B. Xu, L.W. Yang, X.L. Wei, J.W. Ding, J.X. Zhong, P.K. Chu, Hierarchical porous nanocomposite architectures from multi-wall carbon nanotube threaded mesoporous $NaTi_2(PO_4)_3$ nanocrystals for high-performance sodium electrodes. J. Power Sources **327**, 580–590 (2016). https://doi.org/10.1016/j.jpowsour.2016.07.089
80. W. Wu, A. Mohamed, J.F. Whitacre, Microwave synthesized $NaTi_2(PO_4)_3$ as an aqueous sodium-ion negative electrode. J. Electrochem. Soc. **160**(3), A497–A504 (2013). https://doi.org/10.1149/2.054303jes
81. J. Liang, K. Fan, Z. Wei, X. Gao, W. Song, J. Ma, Porous $NaTi_2(PO_4)_3$@C nanocubes as improved anode for sodium-ion batteries. Mater. Res. Bull. **99**, 343–348 (2018). https://doi.org/10.1016/j.materresbull.2017.11.030
82. G. Hasegawa, K. Kanamori, N. Kannari, J.-I. Ozaki, K. Nakanishi, T. Abe, Studies on electrochemical sodium storage into hard carbons with binder-free monolithic electrodes. J. Power Sources **318**, 41–48 (2016). https://doi.org/10.1016/j.jpowsour.2016.04.013
83. N. Hao, R. Hua, S. Chen, Y. Zhang, Z. Zhou, J. Qian, Q. Liu, K.J.B. Wang, Bioelectronics. Multiple signal-amplification via ag and TiO_2 decorated 3D nitrogen doped graphene hydrogel for fabricating sensitive label-free photoelectrochemical thrombin aptasensor. Biosens. Bioelectron. **101**, 14–20 (2018). https://doi.org/10.1016/j.bios.2017.10.014
84. J. Yang, H. Wang, P. Hu, J. Qi, L. Guo, L. Wang, A high-rate and ultralong-life sodium-ion battery based on $NaTi_2(PO_4)_3$ nanocubes with synergistic coating of carbon and rutile TiO_2. Small **11**(31), 3744–3749 (2015). https://doi.org/10.1002/smll.201500144
85. Y. Jiang, J. Shi, M. Wang, L. Zeng, L. Gu, Y. Yu, Highly reversible and ultrafast sodium storage in $NaTi_2(PO_4)_3$ nanoparticles embedded in nanocarbon networks. ACS Appl. Mater. Interfaces. **8**(1), 689–695 (2016). https://doi.org/10.1021/acsami.5b09811
86. L. Wang, B. Wang, G. Liu, T. Liu, T. Gao, D. Wang, Carbon nanotube decorated $NaTi_2(PO_4)_3$/C nanocomposite for a high-rate and low-temperature sodium-ion battery anode. RSC Adv. **6**(74), 70277–70283 (2016). https://doi.org/10.1039/c6ra11042h
87. M. Bian, L. Tian, Design and synthesis of three-dimensional $NaTi_2(PO_4)_3$@CNT microspheres as advanced anode materials for rechargeable sodium-ion batteries. Ceram. Int. **43**(12), 9543–9546 (2017). https://doi.org/10.1016/j.ceramint.2017.04.029
88. Z. Zhou, N. Li, C. Zhang, X. Chen, F. Xu, C. Peng, Preparation of carbon layer and carbon nanotube co-decorated $NaTi_2(PO_4)_3$ anode and its application in sodium-ion batteries. Solid State Ion. **324**, 87–91 (2018). https://doi.org/10.1016/j.ssi.2018.06.011
89. X. Li, P. Yan, M.H. Engelhard, A.J. Crawford, V.V. Viswanathan, C. Wang, J. Liu, V.L. Sprenkle, The importance of solid electrolyte interphase formation for long cycle stability

 https://doi.org/10.1007/s40820-019-0273-1

full-cell Na-ion batteries. Nano Energy **27**, 664–672 (2016). https://doi.org/10.1016/j.nanoen.2016.07.030

90. B. Zhang, R. Dugas, G. Rousse, P. Rozier, A.M. Abakumov, J.-M. Tarascon, Insertion compounds and composites made by ball milling for advanced sodium-ion batteries. Nat. Commun. **7**, 10308 (2016). https://doi.org/10.1038/ncomms10308
91. S. Guo, H. Yu, P. Liu, Y. Ren, T. Zhang, M. Chen, M. Ishida, H. Zhou, High-performance symmetric sodium-ion batteries using a new, bipolar O_3-type material, $Na_{0.8}Ni_{0.4}Ti_{0.6}O_2$. Energy Environ. Sci. **8**(4), 1237–1244 (2015). https://doi.org/10.1039/c4ee03361b
92. J.-Y. Hwang, S.-T. Myung, J.-H. Lee, A. Abouimrane, I. Belharouak, Y.-K. Sun, Ultrafast sodium storage in anatase TiO_2 nanoparticles embedded on carbon nanotubes. Nano Energy **16**, 218–226 (2015). https://doi.org/10.1016/j.nanoen.2015.06.017
93. H. Wang, Y. Xiao, C. Sun, C. Lai, X. Ai, A type of sodium-ion full-cell with a layered $NaNi_{0.5}Ti_{0.5}O_2$ cathode and a pre-sodiated hard carbon anode. RSC Adv. **5**(129), 106519–106522 (2015). https://doi.org/10.1039/c5ra21235a
94. D. Yang, X. Sun, K. Lim, R.R. Gaddam, N.A. Kumar, K. Kang, X.S. Zhao, Pre-sodiated nickel cobaltite for high-performance sodium-ion capacitors. J. Power Sources **362**, 358–365 (2017). https://doi.org/10.1016/j.jpowsour.2017.07.053
95. H. Zhang, B. Qin, D. Buchholz, S. Passerini, High-efficiency sodium-ion battery based on NASICON electrodes with high power and long lifespan. ACS Appl. Energy Mater. (2018). https://doi.org/10.1021/acsaem.1028b01390
96. J. Peng, J. Wang, H. Yi, W. Hu, Y. Yu et al., A dual-insertion type sodium-ion full cell based on high-quality ternary-metal prussian blue analogs. Adv. Energy Mater. **8**(11), 1702856 (2018). https://doi.org/10.1002/aenm.201702856
97. X. Li, X. Zhu, J. Liang, Z. Hou, Y. Wang, N. Lin, Y. Zhu, Y. Qian, Graphene-supported $NaTi_2(PO_4)_3$ as a high rate anode material for aqueous sodium ion batteries. J. Electrochem. Soc. **161**(6), A1181–A1187 (2014). https://doi.org/10.1149/2.0081409jes
98. F. Bonaccorso, L. Colombo, G. Yu, M. Stoller, V. Tozzini, A.C. Ferrari, R.S. Ruoff, V. Pellegrini, Graphene, related two-dimensional crystals, and hybrid systems for energy conversion and storage. Science **347**(6217), 1246501 (2015). https://doi.org/10.1126/science.1246501
99. X. Li, L. Zhi, Graphene hybridization for energy storage applications. Chem. Soc. Rev. **47**(9), 3189–3216 (2018). https://doi.org/10.1039/C7CS00871F
100. H. Zhang, M. Chhowalla, Z. Liu, 2D nanomaterials: graphene and transition metal dichalcogenides. Chem. Soc. Rev. **47**(9), 3015–3017 (2018). https://doi.org/10.1039/C8CS90048E
101. J. Huang, Z. Wei, J. Liao, W. Ni, C. Wang, J. Ma, Molybdenum and tungsten chalcogenides for lithium/sodium-ion batteries: beyond MoS_2. J. Energy Chem. **33**, 100–124 (2018). https://doi.org/10.1016/j.jechem.2018.1009.1001
102. G. Nyström, A. Marais, E. Karabulut, L. Wågberg, Y. Cui, M.M. Hamedi, Self-assembled three-dimensional and compressible interdigitated thin-film supercapacitors and batteries. Nat. Commun. **6**, 7259 (2015). https://doi.org/10.1038/ncomms8259
103. P. Simon, Y. Gogotsi, Materials for electrochemical capacitors. Nat. Mater. **7**, 845 (2008). https://doi.org/10.1038/nmat2297
104. Y. Hu, X. Ma, P. Guo, F. Jaeger, Z. Wang, Design of $NaTi_2(PO_4)_3$ nanocrystals embedded in N-doped graphene sheets for sodium-ion battery anode with superior electrochemical performance. Ceram. Int. **43**(15), 12338–12342 (2017). https://doi.org/10.1016/j.ceramint.2017.06.098
105. Y. Zuo, L. Chen, Z. Zuo, Y. Huang, X. Liu, Rational construction of $NaTi_2(PO_4)_3$@C nanocrystals embedded in graphene sheets as anode materials for Na-ion batteries. Ceram. Int. **43**(15), 12915–12919 (2017). https://doi.org/10.1016/j.ceramint.2017.06.189
106. H.-K. Roh, H.-K. Kim, M.-S. Kim, D.-H. Kim, K.Y. Chung, K.C. Roh, K.-B. Kim, In situ synthesis of chemically bonded $NaTi_2(PO_4)_3$/rGO 2D nanocomposite for high-rate sodium-ion batteries. Nano Res. **9**(6), 1844–1855 (2016). https://doi.org/10.1007/s12274-016-1077-y
107. Z. Wang, J. Liang, K. Fan, X. Liu, C. Wang, J. Ma, Porous $NaTi_2(PO_4)_3$ nanocubes anchored on porous carbon nanosheets for high performance sodium-ion batteries. Front. Chem. **6**, 396 (2018). https://doi.org/10.3389/fchem.2018.00396
108. Y. Zhong, X. Xia, F. Shi, J. Zhan, J. Tu, H.J. Fan, Transition metal carbides and nitrides in energy storage and conversion. Adv. Sci. **3**(5), 1500286 (2016). https://doi.org/10.1002/advs.201500286
109. B. Anasori, M.R. Lukatskaya, Y. Gogotsi, 2D metal carbides and nitrides (MXenes) for energy storage. Nat. Rev. Mater. **2**(2), 16098 (2017). https://doi.org/10.1038/natrevmats.2016.98
110. Q. Yang, T. Jiao, M. Li, Y. Li, L. Ma et al., In situ formation of $NaTi_2(PO_4)_3$ cubes on Ti_3C_2 Mxene for dual-mode sodium storage. J. Mater. Chem. A **6**(38), 18525–18532 (2018). https://doi.org/10.1039/C8TA06995F
111. C. Yang, X. Sun, Y.R. Zhang, Y. Liu, Q.A. Zhang, C.Z. Yuan, Facile synthesis of hierarchical $NaTi_2(PO_4)_3$/Ti_3C_2 nanocomposites with superior sodium storage performance. Mater. Lett. **236**, 408–411 (2019). https://doi.org/10.1016/j.matlet.2018.10.147
112. D. Guo, J. Qin, C. Zhang, M. Cao, Constructing flexible and binder-free $NaTi_2(PO_4)_3$ film electrode with a sandwich structure by a two-step graphene hybridizing strategy as an ultrastable anode for long-life sodium-ion batteries. Cryst. Growth Des. **18**(6), 3291–3301 (2018). https://doi.org/10.1021/acs.cgd.7b01549
113. L. Xu, G. Xu, Z. Chen, X. Wei, J. Cao, L. Yang, 3D nanocomposite archiecture constructed by reduced graphene oxide, thermally-treated protein and mesoporous $NaTi_2(PO_4)_3$ nanocrystals as free-standing electrodes for advanced sodium ion battery. J. Mater. Sci.-Mater. Electron. **29**(11), 9258–9267 (2018). https://doi.org/10.1007/s10854-018-8955-x

114. G. Xu, Z. Li, X. Wei, L. Yang, P.K. Chu, Monolithic hierarchical carbon assemblies embedded with mesoporous $NaTi_2(PO_4)_3$ nanocrystals for flexible high-performance sodium anodes. Electrochim. Acta **254**, 328–336 (2017). https://doi.org/10.1016/j.electacta.2017.09.121
115. Z. Wang, H. Li, Z. Tang, Z. Liu, Z. Ruan, L. Ma, Q. Yang, D. Wang, C. Zhi, Hydrogel electrolytes for flexible aqueous energy storage devices. Adv. Funct. Mater. **28**, 1804560 (2018). https://doi.org/10.1002/adfm.201804560
116. M.-I. Jamesh, Recent advances on flexible electrodes for Na-ion batteries and Li–S batteries. J. Energy Chem. **32**, 15–44 (2018). https://doi.org/10.1016/j.jechem.2018.06.011
117. Z. Guo, Y. Zhao, Y. Ding, X. Dong, L. Chen et al., Multifunctional flexible aqueous sodium-ion batteries with high safety. Chem **3**(2), 348–362 (2017). https://doi.org/10.1016/j.chempr.2017.05.004
118. D. Guo, J. Qin, Z. Yin, J. Bai, Y.-K. Sun, M. Cao, Achieving high mass loading of $Na_3V_2(PO_4)_3$@carbon on carbon cloth by constructing three-dimensional network between carbon fibers for ultralong cycle-life and ultrahigh rate sodium-ion batteries. Nano Energy **45**, 136–147 (2018). https://doi.org/10.1016/j.nanoen.2017.12.038
119. G. Xu, L. Yang, Z. Li, X. Wei, P.K. Chu, Protein-assisted assembly of mesoporous nanocrystals and carbon nanotubes for self-supporting high-performance sodium electrodes. J. Mater. Chem. A **5**(6), 2749–2758 (2017). https://doi.org/10.1039/c6ta09673e
120. L. Fan, S. Wei, S. Li, Q. Li, Y. Lu, Recent progress of the solid-state electrolytes for high-energy metal-based batteries. Adv. Energy Mater. **8**(11), 1702657 (2018). https://doi.org/10.1002/aenm.201702657
121. C. Zhao, L. Liu, X. Qi, Y. Lu, F. Wu, J. Zhao, Y. Yu, Y.S. Hu, L. Chen, Solid-state sodium batteries. Adv. Energy Mater. **8**(17), 1703012 (2018). https://doi.org/10.1002/aenm.201703012
122. A. Hayashi, K. Noi, A. Sakuda, M. Tatsumisago, Superionic glass-ceramic electrolytes for room-temperature rechargeable sodium batteries. Nat. Commun. **3**, 856 (2012). https://doi.org/10.1038/ncomms1843
123. H. Hou, Q. Xu, Y. Pang, L. Li, J. Wang, C. Zhang, C. Sun, Efficient storing energy harvested by triboelectric nanogenerators using a safe and durable all-solid-state sodium-ion battery. Adv. Sci. **4**(8), 1700072 (2017). https://doi.org/10.1002/advs.201700072
124. R. Gao, R. Tan, L. Han, Y. Zhao, Z. Wang, L. Yang, F. Pan, Nanofiber networks of $Na_3V_2(PO_4)_3$ as a cathode material for high performance all-solid-state sodium-ion batteries. J. Mater. Chem. A **5**(11), 5273–5277 (2017). https://doi.org/10.1039/c7ta00314e
125. K. Vignarooban, R. Kushagra, A. Elango, P. Badami, B.-E. Mellander, X. Xu, T. Tucker, C. Nam, A. Kannan, Current trends and future challenges of electrolytes for sodium-ion batteries. Int. J. Hydrogen Energy **41**(4), 2829–2846 (2016). https://doi.org/10.1016/j.ijhydene.2015.12.090
126. K. Zhao, Y. Liu, S. Zhang, S. He, N. Zhang, J. Yang, Z. Zhan, A room temperature solid-state rechargeable sodium ion cell based on a ceramic Na–β″-Al_2O_3 electrolyte and $NaTi_2(PO_4)_3$ cathode. Electrochem. Commun. **69**, 59–63 (2016). https://doi.org/10.1016/j.elecom.2016.06.003
127. X. Jiang, Z. Zeng, L. Xiao, X. Ai, H. Yang, Y. Cao, An all-phosphate and zero-strain sodium-ion battery based on $Na_3V_2(PO_4)_3$ cathode, $NaTi_2(PO_4)_3$ anode, and trimethyl phosphate electrolyte with intrinsic safety and long lifespan. ACS Appl. Mater. Interfaces **9**(50), 43733–43738 (2017). https://doi.org/10.1021/acsami.7b14946
128. D. Bin, F. Wang, A.G. Tamirat, L. Suo, Y. Wang, C. Wang, Y. Xia, Progress in aqueous rechargeable sodium-ion batteries. Adv. Energy Mater. **8**, 1703008 (2018). https://doi.org/10.1002/aenm.201703008
129. A. Ponrouch, D. Monti, A. Boschin, B. Steen, P. Johansson, M. Palacin, Non-aqueous electrolytes for sodium-ion batteries. J. Mater. Chem. A **3**(1), 22–42 (2015). https://doi.org/10.1039/c4ta04428b
130. Z. Zeng, X. Jiang, R. Li, D. Yuan, X. Ai, H. Yang, Y. Cao, A safer sodium-ion battery based on nonflammable organic phosphate electrolyte. Adv. Sci. **3**(9), 1600066 (2016). https://doi.org/10.1002/advs.201600066
131. S. Yu, Z. Liu, H. Tempel, H. Kungl, R.-A. Eichel, Self-standing nasicon-type electrodes with high mass loading for fast-cycling all-phosphate sodium-ion batteries. J. Mater. Chem. A **6**(37), 18304–18317 (2018). https://doi.org/10.1039/c8ta07313a
132. E. Ventosa, D. Buchholz, S. Klink, C. Flox, L.G. Chagas, C. Vaalma, W. Schuhmann, S. Passerini, J.R. Morante, Non-aqueous semi-solid flow battery based on Na-ion chemistry. P2-type $Na_xNi_{0.22}Co_{0.11}Mn_{0.66}O_2$-$NaTi_2(PO_4)_3$. Chem. Commun. **51**(34), 7298–7301 (2015). https://doi.org/10.1039/c4cc09597a
133. M. Wu, Y. Wang, Z. Wei, L. Wang, M. Zhuo, J. Zhang, X. Han, J. Ma, Ternary doped porous carbon nanofibers with excellent ORR and OER performance for zinc–air batteries. J. Mater. Chem. A **6**(23), 10918–10925 (2018). https://doi.org/10.1039/c8ta02416b
134. F.E. Mouahid, M. Bettach, M. Zahir, P. Maldonado-Manso, S. Bruque, E.R. Losilla, M.A.G. Aranda, Crystal chemistry and ion conductivity of the $Na_x^{1+}Ti_x^{2-}Al_x(PO_4)_3$ ($0 \le x \le 0.9$) NASICON series. J. Mater. Chem. **10**(12), 2748–2757 (2000). https://doi.org/10.1039/b004837m
135. M.J. Aragón, C. Vidal-Abarca, P. Lavela, J.L. Tirado, High reversible sodium insertion into iron substituted $Na_x^{1+}Ti_x^{2-}Fe_x(PO_4)_3$. J. Power Sources **252**, 208–213 (2014). https://doi.org/10.1016/j.jpowsour.2013.12.006
136. S. Difi, I. Saadoune, M.T. Sougrati, R. Hakkou, K. Edstrom, P.-E. Lippens, Role of iron in $Na_{1.5}Fe_{0.5}Ti_{1.5}(PO_4)_3$/C as electrode material for Na-ion batteries studied by operando mössbauer spectroscopy. Hyperfine Interact. **237**(1), 61 (2016). https://doi.org/10.1007/s10751-016-1292-7
137. S. Difi, I. Saadoune, M.T. Sougrati, R. Hakkou, K. Edstrom, P.-E. Lippens, Mechanisms and performances of $Na_{1.5}Fe_{0.5}Ti_{1.5}(PO_4)_3$/C composite as electrode material for Na-ion batteries. J. Phys. Chem. C **119**(45), 25220–25234 (2015). https://doi.org/10.1021/acs.jpcc.5b07931

 https://doi.org/10.1007/s40820-019-0273-1

138. H. Gao, J.B. Goodenough, An aqueous symmetric sodium-ion battery with NASICON-structured $Na_3MnTi(PO_4)_3$. Angew. Chem. Int. Ed. **55**(41), 12768–12772 (2016). https://doi.org/10.1002/anie.201606508
139. Z. Jiang, J. Zhu, Y. Li, Z. He, W. Meng, Y. Jiang, L. Dai, L. Wang, Effect of Sn doping on the electrochemical performance of $NaTi_2(PO_4)_3$/C composite. Ceram. Intern. **44**(13), 15646–15652 (2018). https://doi.org/10.1016/j.ceramint.2018.05.233
140. F. Zhang, W. Li, X. Xiang, M. Sun, Nanocrystal-assembled porous $Na_3MgTi(PO_4)_3$ aggregates as highly stable anode for aqueous sodium-ion batteries. Chemistry **23**(52), 12944–12948 (2017). https://doi.org/10.1002/chem.201703044
141. J.-Y. Luo, W.-J. Cui, P. He, Y.-Y. Xia, Raising the cycling stability of aqueous lithium-ion batteries by eliminating oxygen in the electrolyte. Nat. Chem. **2**(9), 760–765 (2010). https://doi.org/10.1038/nchem.763
142. H. Kim, J. Hong, K.-Y. Park, H. Kim, S.-W. Kim, K. Kang, Aqueous rechargeable Li and Na ion batteries. Chem. Rev. **114**(23), 11788–11827 (2014). https://doi.org/10.1021/cr500232y
143. Y. Wang, J. Liu, B. Lee, R. Qiao, Z. Yang et al., Ti-substituted tunnel-type $Na_{0.44}MnO_2$ oxide as a negative electrode for aqueous sodium-ion batteries. Nat. Commun. **6**, 6401 (2015). https://doi.org/10.1038/ncomms7401
144. H. Pan, Y.-S. Hu, L. Chen, Room-temperature stationary sodium-ion batteries for large-scale electric energy storage. Energy Environ. Sci. **6**(8), 2338–2360 (2013). https://doi.org/10.1039/C3EE40847G
145. Y. You, Z. Sang, J. Liu, Recent developments on aqueous sodium-ion batteries. Mater. Technol. **31**(9), 501–509 (2016). https://doi.org/10.1080/10667857.2016.1189709
146. F. Sagane, Synthesis of $NaTi_2(PO_4)_3$ thin-film electrodes by sol–gel method and study on the kinetic behavior of Na^+-ion insertion/extraction reaction in aqueous solution. J. Electrochem. Soc. **163**(13), A2835–A2839 (2016). https://doi.org/10.1149/2.0161614jes
147. K. Nakamoto, Y. Kano, A. Kitajou, S. Okada, Electrolyte dependence of the performance of a $Na_2FeP_2O_7/NaTi_2(PO_4)_3$ rechargeable aqueous sodium-ion battery. J. Power Sources **327**, 327–332 (2016). https://doi.org/10.1016/j.jpowsour.2016.07.052
148. A.I. Mohamed, N.J. Sansone, B. Kuei, N.R. Washburn, J.E. Whitacre, Using polypyrrole coating to improve cycling stability of $NaTi_2(PO_4)_3$ as an aqueous Na-ion anode. J. Electrochem. Soc. **162**(10), A2201–A2207 (2015). https://doi.org/10.1149/2.0961510jes
149. X. Zhan, M. Shirpour, Evolution of solid/aqueous interface in aqueous sodium-ion batteries. Chem. Commun. **53**(1), 204–207 (2017). https://doi.org/10.1039/c6cc08901a
150. Y. He, Y. Hua, Y. Wu, C. Chi, Y. Shi, C. Ai, $NaTi_2(PO_4)_3$/carbon and $NaTi_2(PO_4)_3$/graphite composites as anode materials for aqueous rechargeable Na-ion batteries. Electrochemistry **84**(9), 705–708 (2016). https://doi.org/10.5796/electrochemistry.84.705
151. X. Cao, Y. Yang, Facile synthesis of $NaTi_2(PO_4)_3$-carbon composite through solid state method and its application in aqueous sodium ion battery. Mater. Lett. **231**, 183–186 (2018). https://doi.org/10.1016/j.matlet.2018.08.020
152. T.-F. Hung, W.-H. Lan, Y.-W. Yeh, W.-S. Chang, C.-C. Yang, J.-C. Lin, Hydrothermal synthesis of sodium titanium phosphate nanoparticles as efficient anode materials for aqueous sodium-ion batteries. ACS Sustain. Chem. Eng. **4**(12), 7074–7079 (2016). https://doi.org/10.1021/acssuschemeng.6b01962
153. X. Yao, Y. Luo, Y. Li, W. Li, M. Fang, M. Shui, J. Shu, Y. Ren, The investigation of $NaTi_2(PO_4)_3$@C/Ag as a high-performance anode material for aqueous rechargeable sodium-ion batteries. Mater. Res. Bull. **104**, 194–201 (2018). https://doi.org/10.1016/j.materresbull.2018.03.035
154. M. Forsyth, H. Yoon, F. Chen, H. Zhu, D.R. MacFarlane, M. Armand, P.C. Howlett, Novel Na^+ ion diffusion mechanism in mixed organic–inorganic ionic liquid electrolyte leading to high Na^+ transference number and stable, high rate electrochemical cycling of sodium cells. J. Phys. Chem. C **120**(8), 4276–4286 (2016). https://doi.org/10.1021/acs.jpcc.5b11746
155. B. Zhao, Q. Wang, S. Zhang, C. Deng, Self-assembled wafer-like porous $NaTi_2(PO_4)_3$ decorated with hierarchical carbon as a high-rate anode for aqueous rechargeable sodium batteries. J. Mater. Chem. A **3**(22), 12089–12096 (2015). https://doi.org/10.1039/c5ta02568k
156. B. Zhao, B. Lin, S. Zhang, C. Deng, A frogspawn-inspired hierarchical porous $NaTi_2(PO_4)_3$–C array for high-rate and long-life aqueous rechargeable sodium batteries. Nanoscale **7**(44), 18552–18560 (2015). https://doi.org/10.1039/c5nr06505d
157. W. Wu, J. Yan, A. Wise, A. Rutt, J.F. Whitacre, Using intimate carbon to enhance the performance of $NaTi_2(PO4)_3$ anode materials: carbon nanotubes vs graphite. J. Electrochem. Soc. **161**(4), A561–A567 (2014). https://doi.org/10.1149/2.059404jes
158. Z. Liu, Y. An, G. Pang, S. Dong, C. Xu, C. Mi, X. Zhang, Tin modified $NaTi_2(PO_4)_3$ as an anode material for aqueous sodium ion batteries. Chem. Eng. J. **353**, 814–823 (2018). https://doi.org/10.1016/j.cej.2018.07.159
159. Z. Hou, X. Li, J. Liang, Y. Zhu, Y. Qian, An aqueous rechargeable sodium ion battery based on a $NaMnO_2$–$NaTi_2(PO_4)_3$ hybrid system for stationary energy storage. J. Mater. Chem. A **3**(4), 1400–1404 (2015). https://doi.org/10.1039/c4ta06018k
160. X. Zhang, Z. Hou, X. Li, J. Liang, Y. Zhu, Y. Qian, Na-birnessite with high capacity and long cycle life for rechargeable aqueous sodium-ion battery cathode electrodes. J. Mater. Chem. A **4**(3), 856–860 (2016). https://doi.org/10.1039/c5ta08857g
161. Y. Liu, Y. Qiao, W. Zhang, H. Wang, K. Chen, H. Zhu, Z. Li, Y. Huang, Nanostructured alkali cation incorporated δ-MnO_2 cathode materials for aqueous sodium-ion batteries. J. Mater. Chem. A **3**(15), 7780–7785 (2015). https://doi.org/10.1039/c5ta00396b

162. Y. Liu, Y. Qiao, W. Zhang, H. Xu, Z. Li, Y. Shen, L. Yuan, X. Hu, X. Dai, Y. Huang, High-performance aqueous sodium-ion batteries with $K_{0.27}MnO_2$ cathode and their sodium storage mechanism. Nano Energy **5**, 97–104 (2014). https://doi.org/10.1016/j.nanoen.2014.02.010
163. Y. Liu, Y. Qiao, X. Lou, X. Zhang, W. Zhang, Y. Huang, Hollow $K_{0.27}MnO_2$ nanospheres as cathode for high-performance aqueous sodium ion batteries. ACS Appl. Mater. Interfaces **8**(23), 14564–14571 (2016). https://doi.org/10.1021/acsami.6b03089
164. X.-Y. Wu, M.-Y. Sun, Y.-F. Shen, J.-F. Qian, Y.-L. Cao, X.-P. Ai, H.-X. Yang, Energetic aqueous rechargeable sodium-ion battery based on $Na_2CuFe(CN)_6$–$NaTi_2(PO_4)_3$ intercalation chemistry. Chemsuschem **7**(2), 407–411 (2014). https://doi.org/10.1002/cssc.201301036
165. G. Pang, P. Nie, C. Yuan, L. Shen, X. Zhang, J. Zhu, B. Ding, Enhanced performance of aqueous sodium-ion batteries using electrodes based on the $NaTi_2(PO_4)_3$/MWNTs–$Na_{0.44}MnO_2$ system. Energy Technol. **2**(8), 705–712 (2014). https://doi.org/10.1002/ente.201402045
166. Y. Wang, L. Mu, J. Liu, Z. Yang, X. Yu, L. Gu, Y.S. Hu, H. Li, X.Q. Yang, L. Chen, A novel high capacity positive electrode material with tunnel-type structure for aqueous sodium-ion batteries. Adv. Energy Mater. **5**(22), 1501005 (2015). https://doi.org/10.1002/aenm.201501005
167. Q. Zhang, C. Liao, T. Zhai, H. Li, A high rate 1.2 V aqueous sodium-ion battery based on all nasicon structured $NaTi_2(PO_4)_3$ and $Na_3V_2(PO_4)_3$. Electrochim. Acta **196**, 470–478 (2016). https://doi.org/10.1016/j.electacta.2016.03.007
168. C.W. Mason, F. Lange, Aqueous ion battery systems using sodium vanadium phosphate stabilized by titanium substitution. ECS Electrochem. Lett. **4**(8), A79–A82 (2015). https://doi.org/10.1149/2.0011508eel
169. A. Fernández-Ropero, D. Saurel, B. Acebedo, T. Rojo, M. Casas-Cabanas, Electrochemical characterization of $NaFePO_4$ as positive electrode in aqueous sodium-ion batteries. J. Power Sources **291**, 40–45 (2015). https://doi.org/10.1016/j.jpowsour.2015.05.006
170. W. Wu, S. Shabhag, J. Chang, A. Rutt, J.F. Whitacre, Relating electrolyte concentration to performance and stability for $NaTi_2(PO_4)_3$/$Na_{0.44}MnO_2$ aqueous sodium-ion batteries. J. Electrochem. Soc. **162**(6), A803–A808 (2015). https://doi.org/10.1149/2.0121506jes
171. K. Nakamoto, R. Sakamoto, M. Ito, A. Kitajou, S. Okada, Effect of concentrated electrolyte on aqueous sodium-ion battery with sodium manganese hexacyanoferrate cathode. Electrochemistry **85**(4), 179–185 (2017). https://doi.org/10.5796/electrochemistry.85.179
172. L. Suo, O. Borodin, Y. Wang, X. Rong, W. Sun et al., "Water-in-salt"electrolyte makes aqueous sodium-ion battery safe, green, and long-lasting. Adv. Energy Mater. **7**(21), 1701189 (2017). https://doi.org/10.1002/aenm.201701189
173. J. Han, H. Zhang, A. Varzi, S. Passerini, Fluorine-free water-in-salt electrolyte for green and low-cost aqueous sodium-ion batteries. ChemSusChem **11**(21), 3704–3707 (2018). https://doi.org/10.1002/cssc.201801930
174. A.I. Mohamed, J.F. Whitacre, Capacity fade of $NaTi_2(PO_4)_3$ in aqueous electrolyte solutions: relating pH increases to long term stability. Electrochim. Acta **235**, 730–739 (2017). https://doi.org/10.1016/j.electacta.2017.03.106
175. H. Zhang, B. Qin, J. Han, S. Passerini, Aqueous/non-aqueous hybrid electrolyte for sodium-ion batteries. ACS Energy Lett. **3**(7), 1769–1770 (2018). https://doi.org/10.1021/acsenergylett.8b00919
176. J.F. Whitacre, S. Shanbhag, A. Mohamed, A. Polonsky, K. Carlisle et al., A polyionic, large-format energy storage device using an aqueous electrolyte and thick-format composite $NaTi_2(PO_4)_3$/activated carbon negative electrodes. Energy Technol. **3**(1), 20–31 (2015). https://doi.org/10.1002/ente.201402127
177. P.R. Kumar, Y.H. Jung, B. Moorthy, D.K. Kim, Effect of electrolyte additives on $NaTi_2(PO_4)_3$–C// $Na_3V_2O_{2x}(PO4)_2F_{3-2x}$-MWCNT aqueous rechargeable sodium ion battery performance. J. Electrochem. Soc. **163**(7), A1484–A1492 (2016). https://doi.org/10.1149/2.0031608jes
178. Y. Kong, J. Sun, L. Gai, X. Ma, J. Zhou, $NaTi_2(PO_4)_3$/C||$LiMn_2O_4$ rechargeable battery operating with Li+/Na^+-mixed aqueous electrolyte exhibits superior electrochemical performance. Electrochim. Acta **255**, 220–229 (2017). https://doi.org/10.1016/j.electacta.2017.10.006
179. S.-Y. Tang, C.-H. Mi, J. Wang, A hybrid aqueous full battery based on $LiMn_2O_4$cathode and $NaTi_2(PO_4)_3$ anode. Chin. J. Inorg. Chem. **34**(7), 1279–1284 (2018). https://doi.org/10.11862/CJIC.2018.155
180. D. Sun, G. Jin, Y. Tang, R. Zhang, X. Xue, X. Huang, H. Chu, H. Wang, $NaTi_2(PO_4)_3$ nanoparticles embedded in carbon matrix as long-lived anode for aqueous lithium ion battery. J. Electrochem. Soc. **163**(7), A1388–A1393 (2016). https://doi.org/10.1149/2.1181607jes
181. M. Yao, J. Zhu, W. Meng, C. Li, C. Li et al., Enhanced lithium storage performance of nanostructured $NaTi_2(PO_4)_3$ decorated by nitrogen-doped carbon. Electrochim. Acta **294**, 226–232 (2019). https://doi.org/10.1016/j.electacta.2018.10.116
182. Z. Huang, M. Yao, Z. Jiang, W. Meng, B. Li et al., Impact of fe doping on performance of $NaTi_2(PO_4)_3$/C anode for aqueous lithium ion battery. Solid State Ionics **327**, 123–128 (2018). https://doi.org/10.1016/j.ssi.2018.10.013
183. Z. Jiang, L. Liu, Y. Li, J. Zhu, C. Li et al., Improved lithium storage performance of $NaTi_2(PO_4)_3$/C composite connected by carbon nanotubes. Solid State Ionics **325**, 189–195 (2018). https://doi.org/10.1016/j.ssi.2018.08.007
184. Z. Zhou, S. Gu, Y. Zhang, F. Wu, N. Zhou, Lithium storage performance improvement of $NaTi_2(PO_4)_3$ with nitrogen-doped carbon derived from polyaniline. J. Alloys Compd. **767**, 745–752 (2018). https://doi.org/10.1016/j.jallcom.2018.07.131
185. A. Rudola, S.A.B. Azmansah, P. Balaya, Communication-$Mg(TFSI)_2$-based hybrid magnesium-sodium electrolyte: case study with $NaTi_2(PO_4)_3$//Mg cell. J. Electrochem. Soc. **165**(5), A1092–A1094 (2018). https://doi.org/10.1149/2.1091805jes

 https://doi.org/10.1007/s40820-019-0273-1

186. C. Liu, X. Wang, W. Deng, C. Li, J. Chen, M. Xue, R. Li, F. Pan, Engineering fast ion conduction and selective cation channels for a high-rate and high-voltage hybrid aqueous battery. Angew. Chem. Int. Ed. **57**(24), 7046–7050 (2018). https://doi.org/10.1002/anie.201800479
187. X. Cao, L. Wang, J. Chen, J. Zheng, A low-cost Mg^{2+}/Na^{+} hybrid aqueous battery. J. Mater. Chem. A **6**(32), 15762–15770 (2018). https://doi.org/10.1039/c8ta04930k
188. L. Niu, L. Chen, J. Zhang, P. Jiang, Z. Liu, Revisiting the open-framework zinc hexacyanoferrate: the role of ternary electrolyte and sodium-ion intercalation mechanism. J. Power Sources **380**, 135–141 (2018). https://doi.org/10.1016/j.jpowsour.2018.01.083
189. F. Yu, S. Zhang, C. Fang, Y. Liu, S. He, J. Xia, J. Yang, N. Zhang, Electrochemical characterization of p2-type layered $Na_{2/3}Ni_{1/4}Mn_{3/4}O_2$ cathode in aqueous hybrid sodium/lithium ion electrolyte. Ceram. Int. **43**(13), 9960–9967 (2017). https://doi.org/10.1016/j.ceramint.2017.05.007
190. P. Jiang, H. Shao, L. Chen, J. Feng, Z. Liu, Ion-selective copper hexacyanoferrate with an open-framework structure enables high-voltage aqueous mixed-ion batteries. J. Mater. Chem. A **5**(32), 16740–16747 (2017). https://doi.org/10.1039/c7ta04172a
191. L. Chen, H. Shao, X. Zhou, G. Liu, J. Jiang, Z. Liu, Water-mediated cation intercalation of open-framework indium hexacyanoferrate with high voltage and fast kinetics. Nat. Commun. **7**, 11982 (2016). https://doi.org/10.1038/ncomms11982
192. L. Chen, L. Zhang, X. Zhou, Z. Liu, Aqueous batteries based on mixed monovalence metal ions: a new battery family. Chemsuschem **7**(8), 2295–2302 (2014). https://doi.org/10.1002/cssc.201402084
193. C. Zhang, D. He, J. Ma, W. Tang, T.D. Waite, Faradaic reactions in capacitive deionization (CDI)—problems and possibilities: a review. Water Res. **128**, 314–330 (2018). https://doi.org/10.1016/j.watres.2017.10.024
194. M.A. Ahmed, S. Tewari, Capacitive deionization: processes, materials and state of the technology. J. Electroanal. Chem. **813**, 178–192 (2018). https://doi.org/10.1016/j.jelechem.2018.02.024
195. S. Porada, R. Zhao, A. van der Wal, V. Presser, P.M. Biesheuvel, Review on the science and technology of water desalination by capacitive deionization. Prog. Mater Sci. **58**(8), 1388–1442 (2013). https://doi.org/10.1016/j.pmatsci.2013.03.005
196. F.A. Al Marzooqi, A.A. Al Ghaferi, I. Saadat, N. Hilal, Application of capacitive deionisation in water desalination: a review. Desalination **342**, 3–15 (2014). https://doi.org/10.1016/j.desal.2014.02.031
197. M.A. Anderson, A.L. Cudero, J. Palma, Capacitive deionization as an electrochemical means of saving energy and delivering clean water. Comparison to present desalination practices: will it compete? Electrochim. Acta **55**(12), 3845–3856 (2010). https://doi.org/10.1016/j.electacta.2010.02.012
198. M.E. Suss, V. Presser, Water desalination with energy storage electrode materials. Joule **2**(1), 10–15 (2018). https://doi.org/10.1016/j.joule.2017.12.010
199. S. Shanbhag, Y. Bootwala, J.F. Whitacre, M.S. Mauter, Ion transport and competition effects on $NaTi_2(PO_4)_3$ and $Na_4Mn_9O_{18}$ selective insertion electrode performance. Langmuir **33**(44), 12580–12591 (2017). https://doi.org/10.1021/acs.langmuir.7b02861
200. T. Ikeshoji, Separation of alkali metal ions by intercalation into a prussian blue electrode. J. Electrochem. Soc. **133**(10), 2108–2109 (1986). https://doi.org/10.1149/1.2108350
201. S. Kim, J. Lee, C. Kim, J. Yoon, $Na_2FeP_2O_7$ as a novel material for hybrid capacitive deionization. Electrochim. Acta **203**, 265–271 (2016). https://doi.org/10.1016/j.electacta.2016.04.056
202. S. Kim, H. Yoon, D. Shin, J. Lee, J. Yoon, Electrochemical selective ion separation in capacitive deionization with sodium manganese oxide. J. Colloid Interf. Sci. **506**, 644–648 (2017). https://doi.org/10.1016/j.jcis.2017.07.054
203. F. Chen, Y. Huang, L. Guo, L. Sun, Y. Wang, H.Y. Yang, Dual-ions electrochemical deionization: a desalination generator. Energy Environ. Sci. **10**(10), 2081–2089 (2017). https://doi.org/10.1039/C7EE00855D
204. Y. Huang, F. Chen, L. Guo, J. Zhang, T. Chen, H.Y. Yang, Low energy consumption dual-ion electrochemical deionization system using $NaTi_2(PO_4)_3$–AgNPs electrodes. Desalination **451**, 241–247 (2019). https://doi.org/10.1016/j.desal.2018.02.006
205. F. Chen, Y. Huang, D. Kong, M. Ding, S. Huang, H.Y. Yang, $NaTi_2(PO_4)_3$–Ag electrodes based desalination battery and energy recovery. FlatChem **8**, 9–16 (2018). https://doi.org/10.1016/j.flatc.2018.02.001
206. L. Wang, C. Mu, H. Li, F. Li, A dual-function battery for desalination and energy storage. Inorg. Chem. Front. **5**(10), 2522–2526 (2018). https://doi.org/10.1039/C8QI00704G
207. D.-H. Nam, K.-S. Choi, Bismuth as a new chloride-storage electrode enabling the construction of a practical high capacity desalination battery. J. Am. Chem. Soc. **139**(32), 11055–11063 (2017). https://doi.org/10.1021/jacs.7b01119
208. Z. Guo, Y. Ma, X. Dong, M. Hou, Y. Wang, Y. Xia, Integrating desalination and energy storage using a saltwater-based hybrid sodium-ion supercapacitor. ChemSusChem **11**(11), 1741–1745 (2018). https://doi.org/10.1002/cssc.201800517
209. H. Li, H. Tang, C. Ma, Y. Bai, J. Alvarado et al., Understanding the electrochemical mechanisms induced by gradient Mg^{2+} distribution of Na-rich $Na_x^{3+}V_{2-x}Mg_x(PO_4)_3/C$ for sodium ion batteries. Chem. Mat. **30**(8), 2498–2505 (2018). https://doi.org/10.1021/acs.chemmater.7b03903
210. J. Zeng, Z. Cao, Y. Yang, Y. Wang, Y. Peng, Y. Zhang, J. Wang, J. Zhao, A long cycle-life Na–Mg hybrid battery with a chlorine-free electrolyte based on Mg $(TFSI)_2$. Electrochim. Acta **284**, 1–9 (2018). https://doi.org/10.1016/j.electacta.2018.07.111
211. Y. Xu, W. Cao, Y. Yin, J. Sheng, Q. An, Q. Wei, W. Yang, L. Mai, Novel $NaTi_2(PO_4)_3$ nanowire clusters as high performance cathodes for Mg–Na hybrid-ion batteries. Nano Energy **55**, 526–533 (2019). https://doi.org/10.1016/j.nanoen.2018.10.064

212. J. Ding, W. Hu, E. Paek, D. Mitlin, Review of hybrid ion capacitors: from aqueous to lithium to sodium. Chem. Rev. **118**(14), 6457–6498 (2018). https://doi.org/10.1021/acs.chemrev.8b00116
213. Y.E. Zhu, L. Yang, J. Sheng, Y. Chen, H. Gu, J. Wei, Z. Zhou, Fast sodium storage in TiO_2@CNT@C nanorods for high-performance Na-ion capacitors. Adv. Energy Mater. **7**(22), 1701222 (2017). https://doi.org/10.1002/aenm.201701222
214. H. Hou, X. Qiu, W. Wei, Y. Zhang, X. Ji, Carbon anode materials for advanced sodium-ion batteries. Adv. Energy Mater. **7**(24), 1602898 (2017). https://doi.org/10.1002/aenm.201602898
215. F. Wang, X. Wang, Z. Chang, X. Wu, X. Liu et al., A quasi-solid-state sodium-ion capacitor with high energy density. Adv. Mater. **27**(43), 6962–6968 (2015). https://doi.org/10.1002/adma.201503097
216. S. Liu, Z. Cai, J. Zhou, A. Pan, S. Liang, Nitrogen-doped TiO_2 nanospheres for advanced sodium-ion battery and sodium-ion capacitor applications. J. Mater. Chem. A **4**(47), 18278–18283 (2016). https://doi.org/10.1039/c6ta08472a
217. E. Lim, H. Kim, C. Jo, J. Chun, K. Ku et al., Advanced hybrid supercapacitor based on a mesoporous niobium pentoxide/carbon as high-performance anode. ACS Nano **8**(9), 8968–8978 (2014). https://doi.org/10.1021/nn501972w
218. S. Zhang, Y. Liu, Q. Han, S. He, N. Zhang, J. Yang, Development and characterization of aqueous sodium-ion hybrid supercapacitor based on $NaTi_2(PO_4)_3$//activated carbon. J. Alloys Compd. **729**, 850–857 (2017). https://doi.org/10.1016/j.jallcom.2017.08.256
219. C. Wang, F. Qiu, H. Deng, X. Zhang, P. He, H. Zhou, Study on the aqueous hybrid supercapacitor based on carbon-coated $NaTi_2(PO_4)_3$ and activated carbon electrode materials. Acta Chim. Sin. **75**(2), 241–246 (2017). https://doi.org/10.6023/a16100523
220. H.-K. Roh, M.-S. Kim, K.Y. Chung, M. Ulaganathan, V. Aravindan, S. Madhavi, K.C. Roh, K.-B. Kim, A chemically bonded $NaTi_2(PO_4)_3$/rGO microsphere composite as a high-rate insertion anode for sodium-ion capacitors. J. Mater. Chem. A **5**(33), 17506–17516 (2017). https://doi.org/10.1039/c7ta05252a
221. T. Wei, G. Yang, C. Wang, Iso-oriented $NaTi_2(PO_4)_3$ mesocrystals as anode material for high-energy and long-durability sodium-ion capacitor. ACS Appl. Mater. Interfaces **9**(37), 31861–31870 (2017). https://doi.org/10.1021/acsami.7b08778
222. J.Z. Guo, P.F. Wang, X.L. Wu, X.H. Zhang, Q. Yan, H. Chen, J.P. Zhang, Y.G. Guo, High-energy/power and low-temperature cathode for sodium-ion batteries: in situ XRD study and superior full-cell performance. Adv. Mater. **29**(33), 1701968 (2017). https://doi.org/10.1002/adma.201701968

 https://doi.org/10.1007/s40820-019-0273-1